CONFIDENTIAL

NACA

RESEARCH MEMORANDUM

INVESTIGATION AT HIGH SUBSONIC SPEEDS OF THE EFFECT OF HORIZONTAL-TAIL LOCATION ON LONGITUDINAL AND LATERAL STABILITY CHARACTERISTICS OF A COMPLETE MODEL HAVING A SWEPTBACK WING IN A HIGH LOCATION

By H. Norman Silvers and Thomas J. King, Jr.

Langley Aeronautical Laboratory
Langley Field, Va.

CLASSIFIED DOCUMENT

NATIONAL ADVISORY COMMITTEE
FOR AERONAUTICS

WASHINGTON

April 18, 1956

CONFIDENTIAL

NATIONAL ADVISORY COMMITTEE FOR AERONAUTICS

RESEARCH MEMORANDUM

INVESTIGATION AT HIGH SUBSONIC SPEEDS OF THE EFFECT OF HORIZONTAL-TAIL LOCATION ON LONGITUDINAL AND LATERAL STABILITY CHARACTERISTICS OF A COMPLETE MODEL HAVING A SWEPTBACK WING IN A HIGH LOCATION

By H. Norman Silvers and Thomas J. King, Jr.

SUMMARY

An investigation was made at high subsonic speeds of the longitudinal and lateral stability characteristics of a complete model having four vertical locations of the horizontal tail and a sweptback wing located in a high position on the fuselage. The wing had 45° of sweepback, an aspect ratio of 4.0, and a taper ratio of 0.3. The results were obtained in the Langley high-speed 7- by 10-foot tunnel at Mach numbers from 0.80 to 0.92.

The results show that longitudinal instability at moderate angles of attack was avoided only by placing the horizontal tail below the wing chord plane. At low lift coefficients, the contribution of the horizontal tail to longitudinal stability was increased as the tail was moved to the high or low positions. At the lowest test Mach number (M = 0.8) the directional stability decreased appreciably with increasing lift coefficient for all horizontal-tail locations. Directional stability at high lift coefficients improved with increasing Mach number, particularly when the horizontal tail was mounted at the top of the vertical tail. At low lift coefficients the contribution of the tail assembly to directional stability was a minimum in a medium position (0.084 wing span above wing chord plane). Moving the horizontal tail from the fuselage center line to the top of the vertical tail resulted in a large increase in effective dihedral, particularly at low lift coefficients.

INTRODUCTION

Many coordinated research programs have been undertaken in flight and wind tunnels to develop the present understanding of aircraft

stability problems at low speeds. The National Advisory Committee for Aeronautics is presently extending available research results to high subsonic and supersonic speeds. In reference 1 are presented the stability characteristics of a model at low speeds with various vertical locations of the wing and horizontal tail. Similar results are presented in reference 2 at supersonic speeds. The results in the present paper were obtained at high subsonic speeds on a model having a 45° sweptback wing located high on the fuselage. The effects of vertical location of the horizontal tail and the various component parts of the model on static longitudinal and lateral stability characteristics are presented.

The purpose of the present paper is to present and discuss briefly the experimental results of this investigation.

COEFFICIENTS AND SYMBOLS

All data are presented about the stability system of axes as shown in figure 1. The pitching-moment coefficients are referred to the quarter chord of the mean aerodynamic chord.

C_L lift coefficient, $\frac{\text{Lift}}{qS}$

C_D drag coefficient, $\frac{\text{Drag}}{qS}$

C_m pitching-moment coefficient, $\frac{\text{Pitching moment}}{qS\bar{c}}$

C_l rolling-moment coefficient, $\frac{\text{Rolling moment}}{qSb}$

C_n yawing-moment coefficient, $\frac{\text{Yawing moment}}{qSb}$

C_Y side-force coefficient, $\frac{\text{Side force}}{qS}$

S wing area, sq ft

$\bar{c}$ wing mean aerodynamic chord, $\frac{2}{S}\int_0^{b/2} c^2 dy$, ft

c local chord parallel to plane of symmetry, ft

b	wing span, ft
q	dynamic pressure, $\frac{\rho V^2}{2}$, lb/sq ft
ρ	mass density of air, slugs/cu ft
V	free-stream velocity, ft/sec
M	Mach number
R	Reynolds number of wing based on $\bar{c}$
α	angle of attack, deg
β	angle of sideslip, deg
$\Lambda_{c/4}$	sweep angle of quarter-chord line, deg
y	spanwise distance from plane of symmetry, ft
z	horizontal-tail height from fuselage center line, positive upward, ft
C_{L_α}	lift-curve slope, $\frac{\partial C_L}{\partial \alpha}$
$C_{m_{C_L}}$	pitching-moment-curve slope, $\frac{\partial C_m}{\partial C_L}$
$\Delta C_{m_{C_L}}$	horizontal-tail contribution to $C_{m_{C_L}}$, $\left(C_{m_{C_L}}\right)_{WFVH} - \left(C_{m_{C_L}}\right)_{WFV}$
ΔC_{Y_β}	tail contribution to C_{Y_β}, $\left(C_{Y_\beta}\right)_{WFVH} - \left(C_{Y_\beta}\right)_{WF}$
ΔC_{n_β}	tail contribution to C_{n_β}, $\left(C_{n_\beta}\right)_{WFVH} - \left(C_{n_\beta}\right)_{WF}$
ΔC_{l_β}	tail contribution to C_{l_β}, $\left(C_{l_\beta}\right)_{WFVH} - \left(C_{l_\beta}\right)_{WF}$
$\frac{\bar{x}}{b}$	longitudinal location of effective tail center of pressure, $\frac{\Delta C_{n_\beta}}{\Delta C_{Y_\beta}}$ at $\alpha = 0^\circ$

$\frac{\bar{z}}{b}$ vertical location of effective tail center of pressure, $\frac{\Delta C_{l_\beta}}{\Delta C_{Y_\beta}}$ at $\alpha = 0^\circ$

Subscripts:

t tip

r root

β denotes partial derivative of a coefficient with respect to sideslip angle; for example, $C_{l_\beta} = \frac{\partial C_l}{\partial \beta}$

0 denotes values of a parameter at zero lift coefficient

$\alpha = 0^\circ$ value at angle of attack of 0°

Designation of model components:

W wing

F fuselage

V vertical tail

V' vertical tail + ventral fin

H horizontal tail

MODEL AND APPARATUS

A three-view drawing and tabulated geometric characteristics of the model are presented in figure 2.

The wing was located in a high position such that the wing upper surface at the plane of symmetry was approximately coincident with the highest point on the fuselage. The wing was mounted with 0° incidence and dihedral. Ordinates of the fuselage are presented in table I.

The four vertical locations of the horizontal tail are illustrated in figure 3 and are designated low, center, medium, and high. These designations are employed herein. The incidence of the horizontal tail in each vertical location was 0°.

The model was sting supported and data were obtained from a six-component strain-gage balance located within the fuselage of the model.

TESTS

Longitudinal tests were made in the Langley high-speed 7- by 10-foot tunnel at constant Mach numbers of 0.80, 0.85, 0.90, and 0.92 and at 0° sideslip through an angle-of-attack range from about -2° to about 23° at the lowest Mach number. Lateral parameters were determined through the angle-of-attack range at sideslip angles of $\pm 4^\circ$. Lateral-parameter data were obtained at the same Mach numbers and over approximately the angle-of-attack range covered in tests at 0° sideslip. Tests were also made at constant angles of attack of approximately 0°, 13°, 16°, and 19° through a range of sideslip angle from about -4° to about 12°. At the highest Mach numbers both the angles of attack and angles of sideslip of the model were restricted for structural reasons.

The investigations were performed on the complete model with four vertical locations of the horizontal tail and with the horizontal tail removed. In addition, lateral-parameter tests were performed on the wing-fuselage combination and on the wing-fuselage combination with the vertical tail plus the ventral fin. It should be noted that the ventral fin was used as a support for the horizontal tail in the low position and, except for a test with the horizontal tail off, was used only for this location of the horizontal tail. Sideslip tests ($-4^\circ \leq \beta \leq 12^\circ$) were performed for two vertical locations (center and high) of the horizontal tail.

The Reynolds number based on the mean aerodynamic chord varied with Mach number as illustrated in figure 4.

CORRECTIONS

Blockage corrections were applied to the results by the method of reference 3. Jet-boundary corrections were applied to the angle of attack and drag by the method of reference 4. The drag coefficients were corrected for a longitudinal pressure gradient that exists in the tunnel.

No sting interference tares were applied to the results. The drag coefficients were adjusted to correspond to a condition of free-stream static pressure at the base of the model.

No attempt was made to correct the results for aeroelastic distortion of the model.

PRESENTATION OF RESULTS

The results of the investigation are presented in the figures which are listed as follows:

DISCUSSION

Longitudinal Characteristics

In figures 5 to 8 are shown the longitudinal characteristics of the model without a horizontal tail and with a horizontal tail in four vertical locations. The pitching-moment results (figs. 7 and 8) show that without a horizontal tail the wing-fuselage combination develops the usual pitch-up tendency to be expected for the wing plan form used. It is to be noticed that the wing-fuselage combination referred to consists of the wing, fuselage, and the vertical tail. Pitch-up occurs near the angle of attack where decreases in lift-curve slope are first indicated (fig. 5).

The vertical location of the horizontal tail has a pronounced effect on the pitch-up characteristics of the wing-fuselage combination. In general, the horizontal tail in the high or the medium vertical location (figs. 7 and 8) does not appear to improve the pitch-up characteristics. The center and low locations of the horizontal tail (0.056b and 0.126b below the wing chord plane, respectively) reduced the pitch-up tendencies of the wing-fuselage combination at all Mach numbers with the best characteristics being shown by the low tail.

The effects of horizontal-tail height on some longitudinal characteristics at zero lift are shown in figure 9. As the tail was raised from the low to the high position, the pitching moment at zero angle of attack varied from a negative value to a positive value, the magnitude of the variation being somewhat greater at $M = 0.90$ than at $M = 0.80$. This variation probably results chiefly from the stream pressure and angularity field induced by the vertical tail and fuselage afterbody. Large effects of horizontal-tail height on the pitching-moment slope $\left(\frac{\partial C_m}{\partial C_L}\right)_0$ and the tail contribution $\Delta\left(\frac{\partial C_m}{\partial C_L}\right)_0$ are indicated in figure 9. An increase in tail contribution to longitudinal stability resulted as the tail was moved either above or below the wing chord plane, apparently because of decreased downwash at the tail plane. When mounted on the fuselage center line, the horizontal tail was approximately 70 percent as effective as when mounted at the top of the vertical tail.

Lateral Characteristics

The lateral stability derivatives (fig. 11) indicate that at the lowest test Mach number ($M = 0.80$) the directional stability of the complete model with the horizontal tail at any of the vertical locations investigated decreased rapidly as the lift coefficient was increased above 0.8. This decrease is a result of a reduction in tail effectiveness, since with the horizontal and vertical tails removed, relatively small variations of C_{n_β} with C_L are indicated (fig. 10). An indication of the effects of increasing the test Mach number from 0.80 to 0.92 is illustrated for center and high tail locations in figure 12. For either tail arrangement, directional stability at the higher lift coefficient was improved as the Mach number increased. The improvements were small for the center tail, but were of such magnitude for the high horizontal tail that at a Mach number of 0.92, C_{n_β} increased continuously over the test lift-coefficient range.

At low lift coefficients, the magnitudes of the directional stability of the complete model and of the tail contribution to directional stability (fig. 13) varied with tail height in much the same manner indicated by previous low-speed tests (ref. 1). The curves in figure 13 have been faired with solid lines only through the range from the center tail location to the high tail with results for the low tail indicated by points faired with a broken curve, since additional fin area had to be added to provide a support for the low horizontal tail. Nevertheless, the results for the low tail seem to follow the trend established by the other tail arrangements. As would be expected from consideration of end-plate effects, the directional stability is a minimum when the horizontal tail is in the medium position and is almost the same as the value with horizontal tail removed (indicated by solid isolated symbols). At Mach

numbers of 0.80 and 0.90 the directional stability of the model with the medium horizontal-tail location was about one-fourth of the directional stability of the high tail arrangement. The tail contribution to the directional stability of the medium tail configuration was about 60 percent of the contribution for the high tail arrangement.

At low lift coefficients, an upward movement of the horizontal tail increases the negative value of both the effective dihedral derivative Cl_β and of the tail contribution to Cl_β. (See fig. 13.) This is indicative of a possible upward movement of the center of the load due to sideslip in addition to the increase in tail effectiveness. Figure 13 shows effective tail centers of pressure as determined from the tail contribution to the stability derivatives. As the horizontal tail is moved from the center to the high position an upward movement of center of pressure equal to 11 percent of the wing span (40 percent of the vertical tail span) is indicated. Only a slight fore and aft movement is shown.

Variations of the lateral coefficients C_Y, C_n, and Cl with sideslip angle are presented in figures 14 to 17 for the complete model having center and high tail locations. In general, the directional stability is somewhat better at moderate angles of sideslip (5° to 10°) than at low sideslip angles for the center tail configuration; the high tail configuration, however, at $\alpha \approx 19^\circ$ becomes directionally unstable above $\beta = 8^\circ$ at $M = 0.80$ and $\beta = 6^\circ$ at $M = 0.85$. The rolling-moment curves also are nonlinear, particularly in the angle-of-attack range from 13° to 16°. In this range, the effective dihedral at the higher sideslip angles is somewhat larger than at low sideslip angles.

CONCLUSIONS

An investigation at high subsonic speeds of the longitudinal and lateral stability characteristics of a complete model with varying vertical location of the horizontal tail and a sweptback wing in a high location on the fuselage indicates the following conclusions:

1. For the model configuration investigated, longitudinal instability at moderate lift ccefficients was avoided only by placing the horizontal tail below the wing chord plane.

2. At low lift coefficients, the contribution of the horizontal tail to longitudinal stability was increased as the horizontal tail was moved to high or low positions. When mounted on the fuselage center line the horizontal tail was 70 percent as effective as when mounted at the top of the vertical tail.

3. At the lowest test Mach number (M = 0.80), the directional stability decreased appreciably at the higher lift coefficients for all horizontal-tail locations. Directional stability at high lift coefficients improved with increasing Mach number, particularly when the horizontal tail was mounted at the top of the vertical tail.

4. At low lift coefficients, the directional stability and the contribution of the tail assembly to directional stability was a minimum when the horizontal tail was mounted in a medium position (0.084 wing span above wing chord plane). For this tail arrangement the directional stability and the contribution of the tail assembly to the directional stability were about 25 and 60 percent, respectively, of that obtained when the horizontal tail was mounted at the top of the vertical tail.

5. As the horizontal tail was moved from the fuselage center line to the top of the vertical tail, the effective center of pressure of the load due to sideslip was raised by an amount equal to 11 percent of the wing span or 40 percent of the vertical-tail span. This change in center of pressure, along with the increased tail effectiveness resulted in a large increase in effective dihedral, particularly at low lift coefficients.

Langley Aeronautical Laboratory,
National Advisory Committee for Aeronautics,
Langley Field, Va., January 30, 1956.

REFERENCES

1. Goodman, Alex: Effects of Wing Position and Horizontal-Tail Position on the Static Stability Characteristics of Models With Unswept and 45° Sweptback Surfaces With Some Reference to Mutual Interference. NACA TN 2504, 1951.

2. Spearman, M. Leroy, Driver, Cornelius, and Hughes, William C.: Investigation of Aerodynamic Characteristics in Pitch and Sideslip of a 45° Sweptback-Wing Airplane Model With Various Vertical Locations of Wing and Horizontal Tail - Basic-Data Presentation, M = 2.01. NACA RM L54L06, 1955.

3. Herriot, John G.: Blockage Corrections for Three-Dimensional-Flow Closed-Throat Wind Tunnels, With Consideration of the Effect of Compressibility. NACA Rep. 995, 1950. (Supersedes NACA RM A7B28.)

4. Gillis, Clarence L., Polhamus, Edward C., and Gray, Joseph L., Jr.: Charts for Determining Jet-Boundary Corrections for Complete Models in 7- by 10-Foot Closed Rectangular Wind Tunnels. NACA WR L-123, 1945. (Formerly NACA ARR L5G31.)

TABLE I.
FUSELAGE ORDINATES

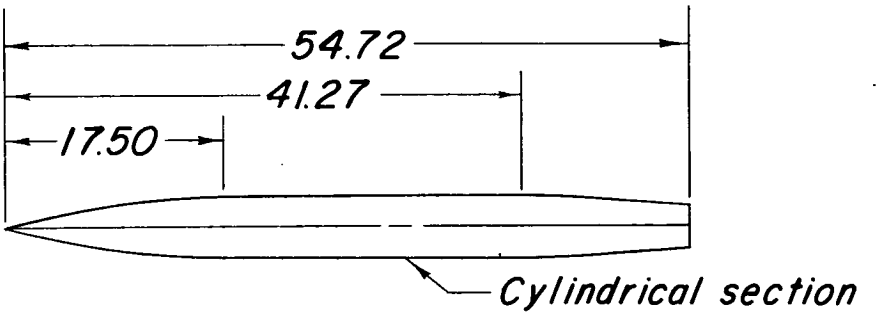

Ordinates, in.

Station	Radius
0	0
2.00	.53
4.00	1.00
6.00	1.44
8.00	1.80
10.00	2.07
12.00	2.30
14.00	2.42
16.00	2.47
17.50	2.50
41.27	2.50
43.27	2.42
45.27	2.35
47.27	2.25
48.30	2.14
54.72	1.65

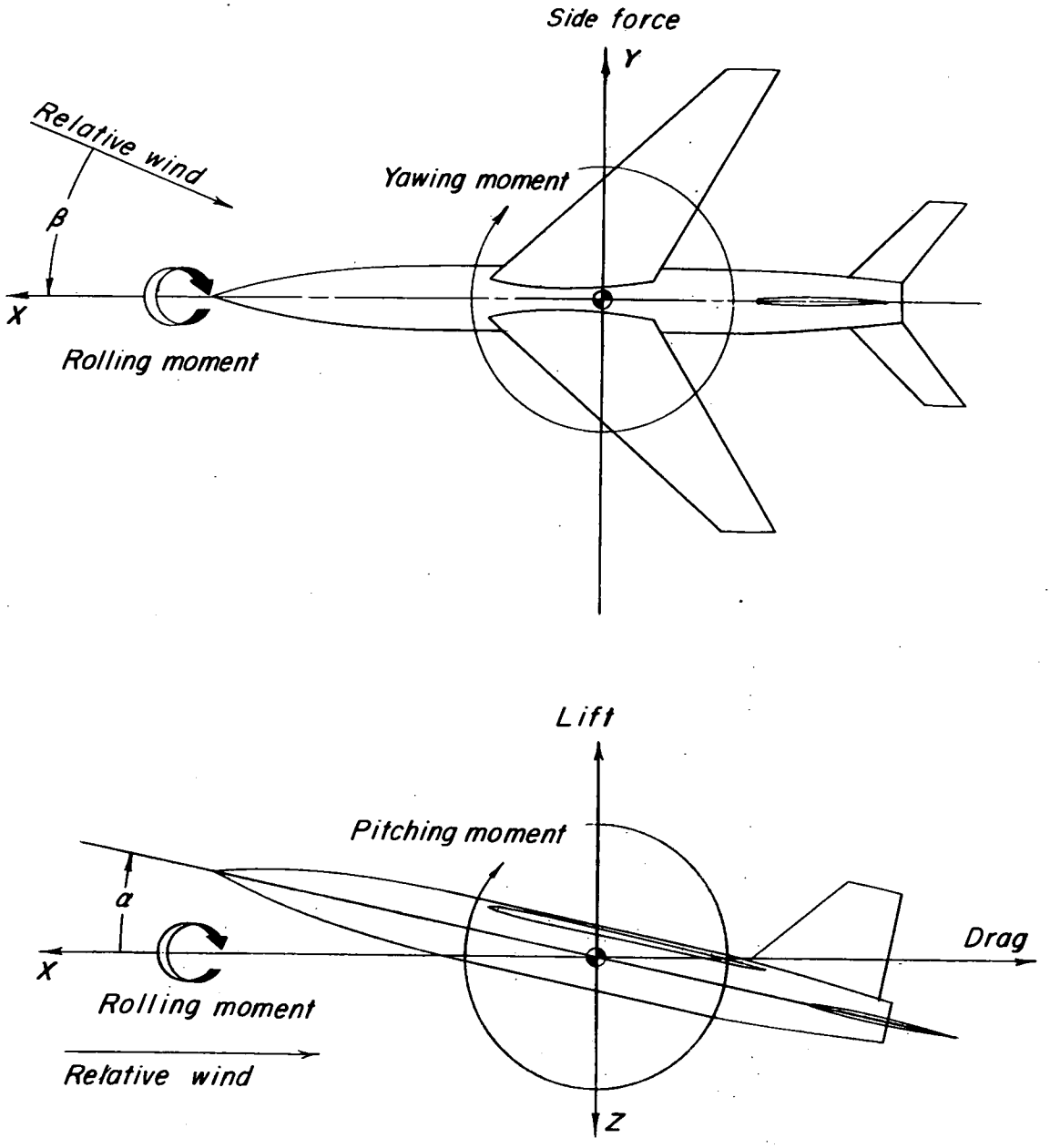

Figure 1.- Stability system of axes. Positive directions of forces, moments, and angles are indicated by arrows.

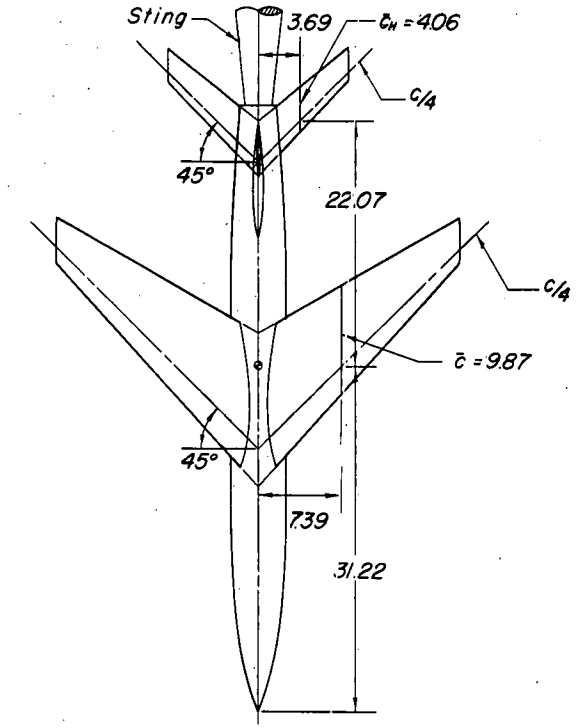

	Model geometry		
	Wing	Horiz. tail	Vert. tail
Area, sq ft	2.25	.451	.612
Aspect ratio	4.00	3.98	1.18
Taper ratio	.30	.603	.411
c_t, in.	4.15	3.04	5.04
c_r, in.	13.85	5.04	12.27
$\Lambda_{c/4}$	45.0°	45.0°	28.0°
NACA airfoil section	65A006	65A006	63A009

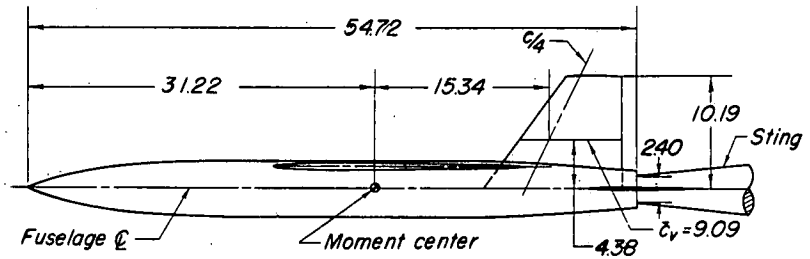

Figure 2.- Three-view drawing of model. All dimensions are in inches except where noted.

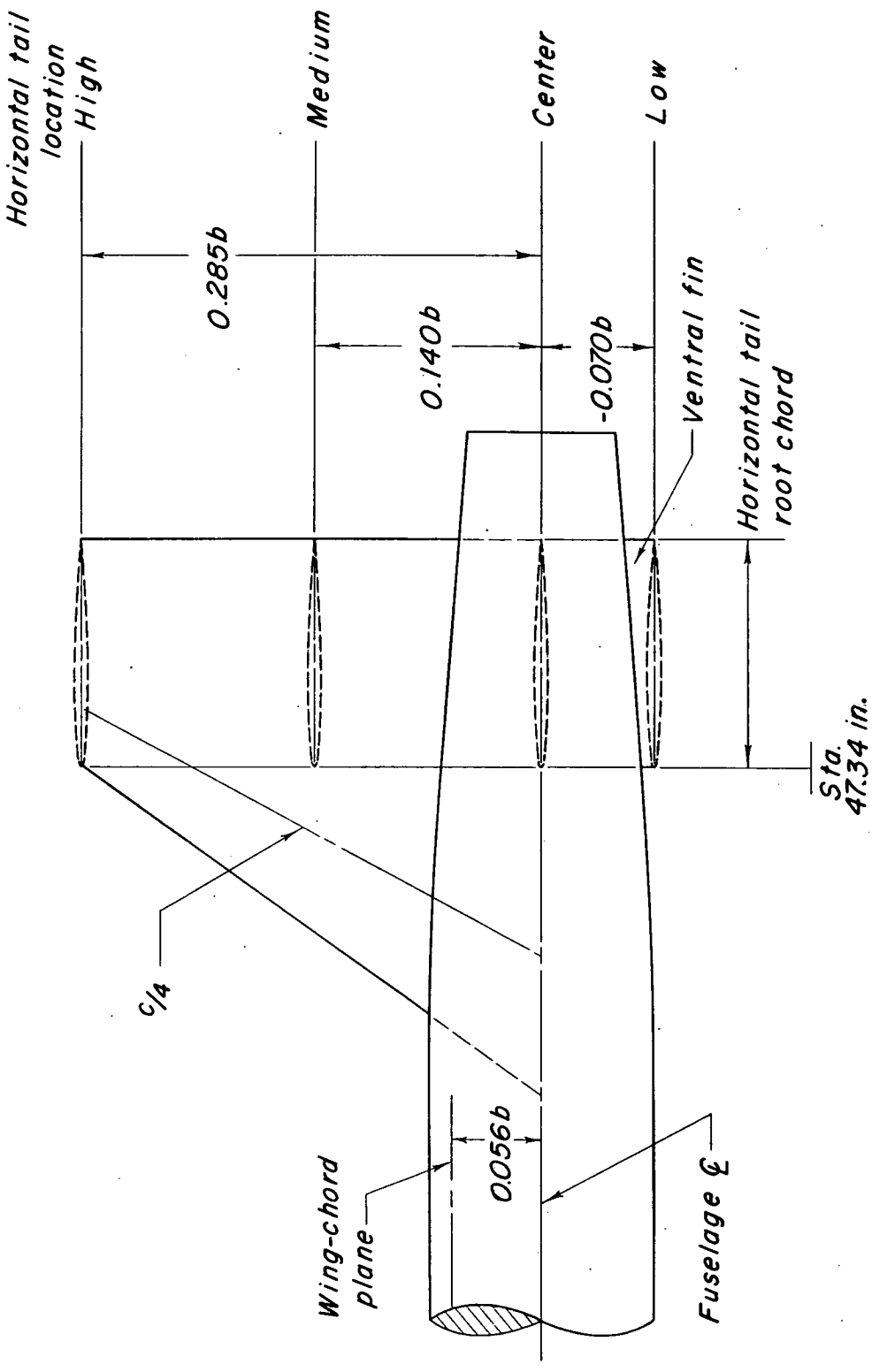

Figure 3.- Locations of the horizontal tail.

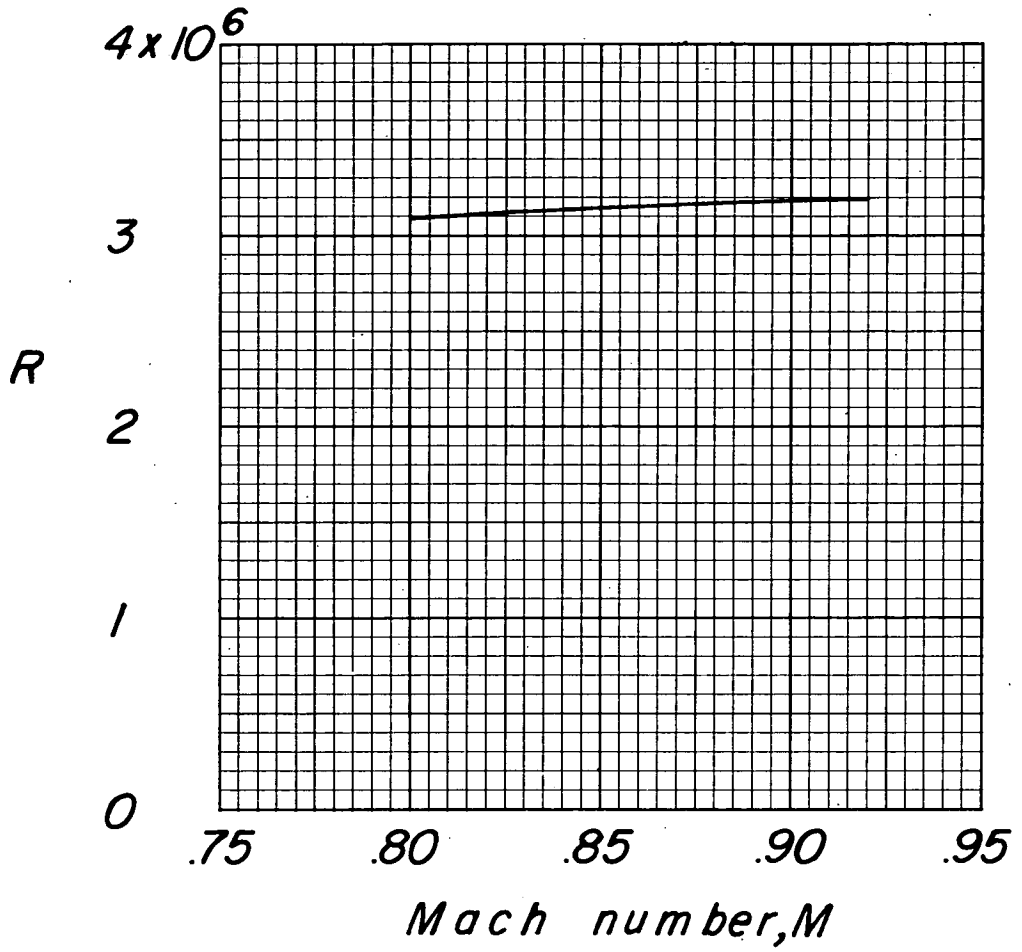

Figure 4.- Variation with Mach number of Reynolds number (based on wing mean aerodynamic chord).

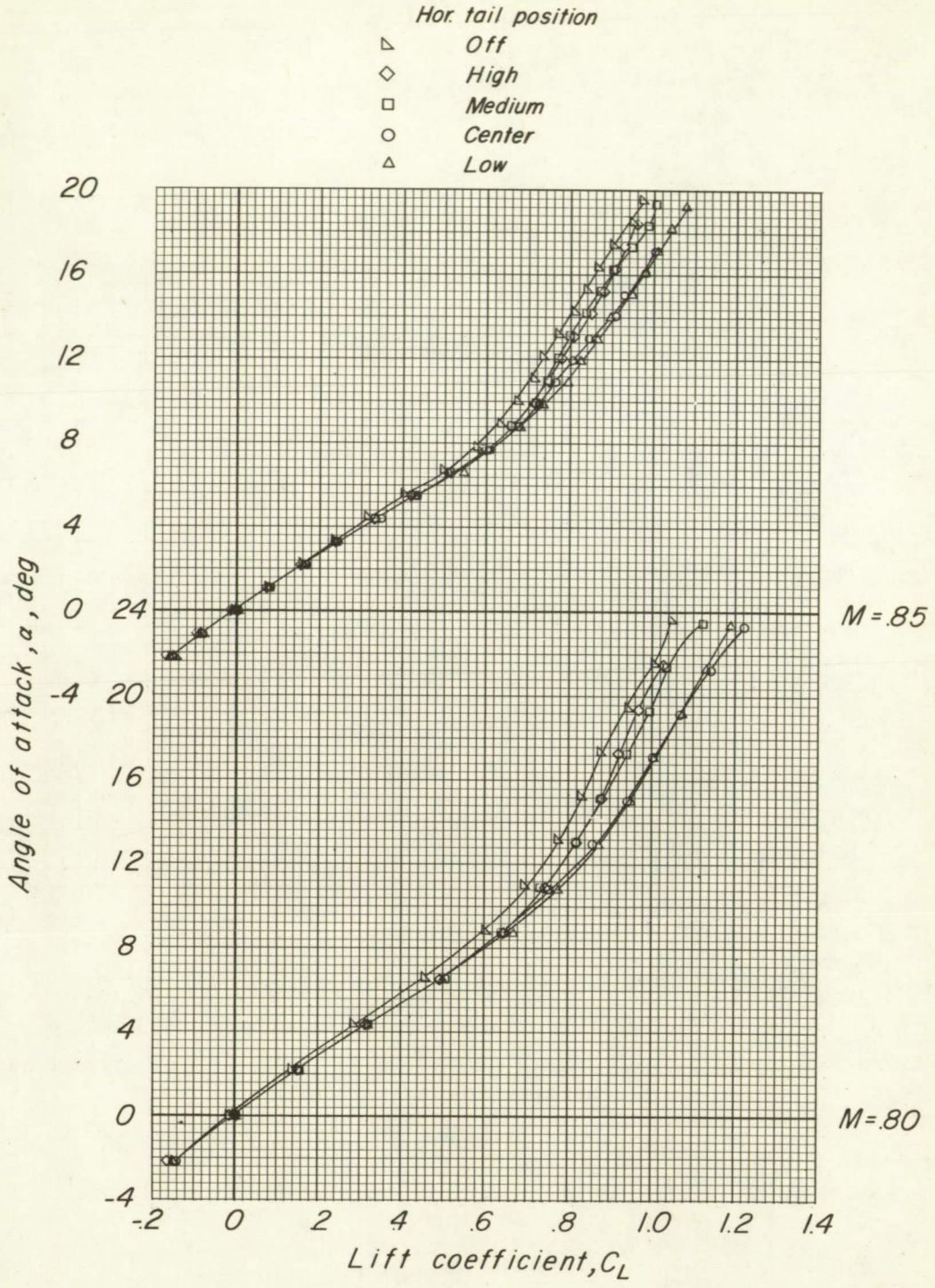

Figure 5.- Variation of lift coefficient with angle of attack of high-wing—fuselage model without and with horizontal tail at various vertical locations.

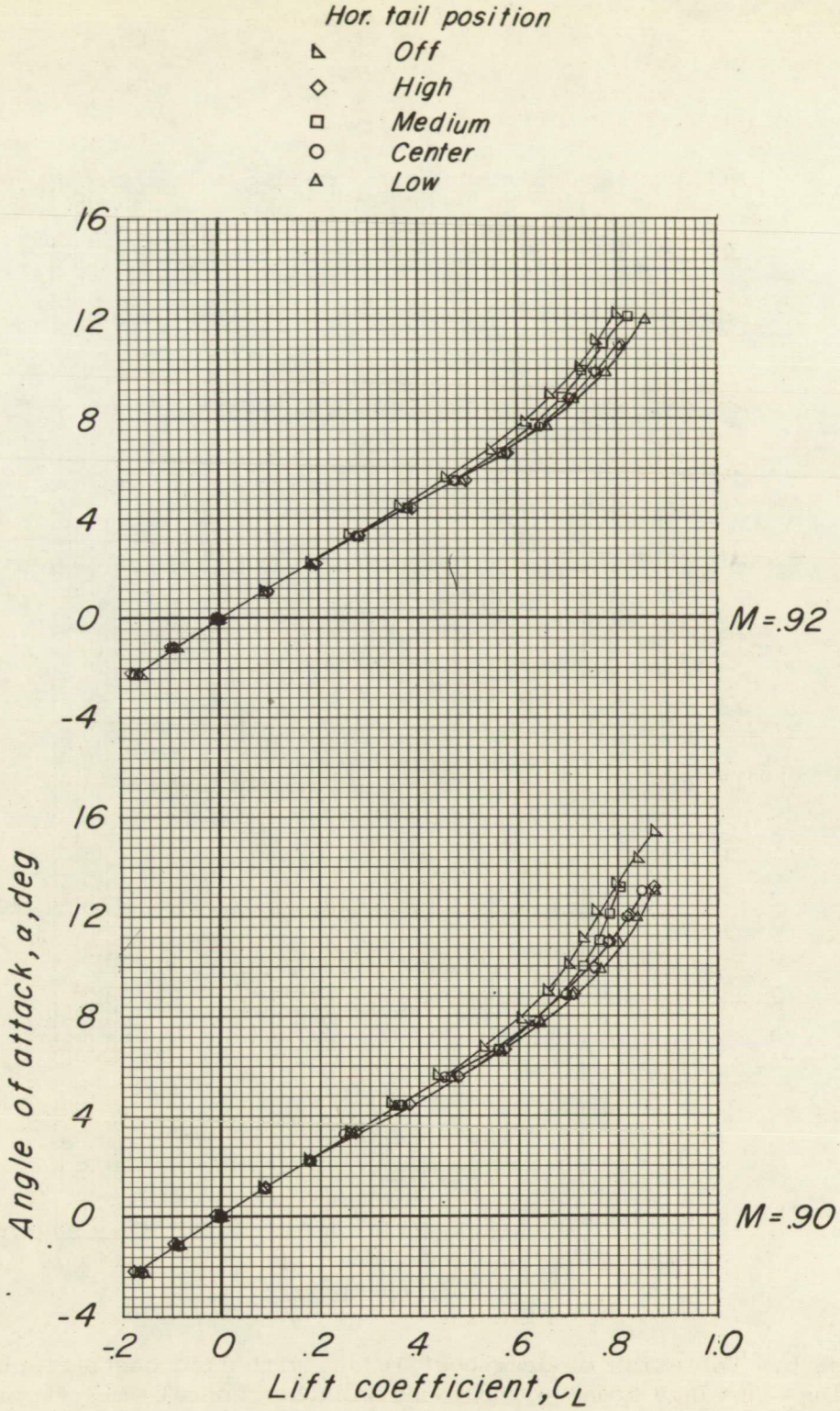

Figure 5.- Concluded.

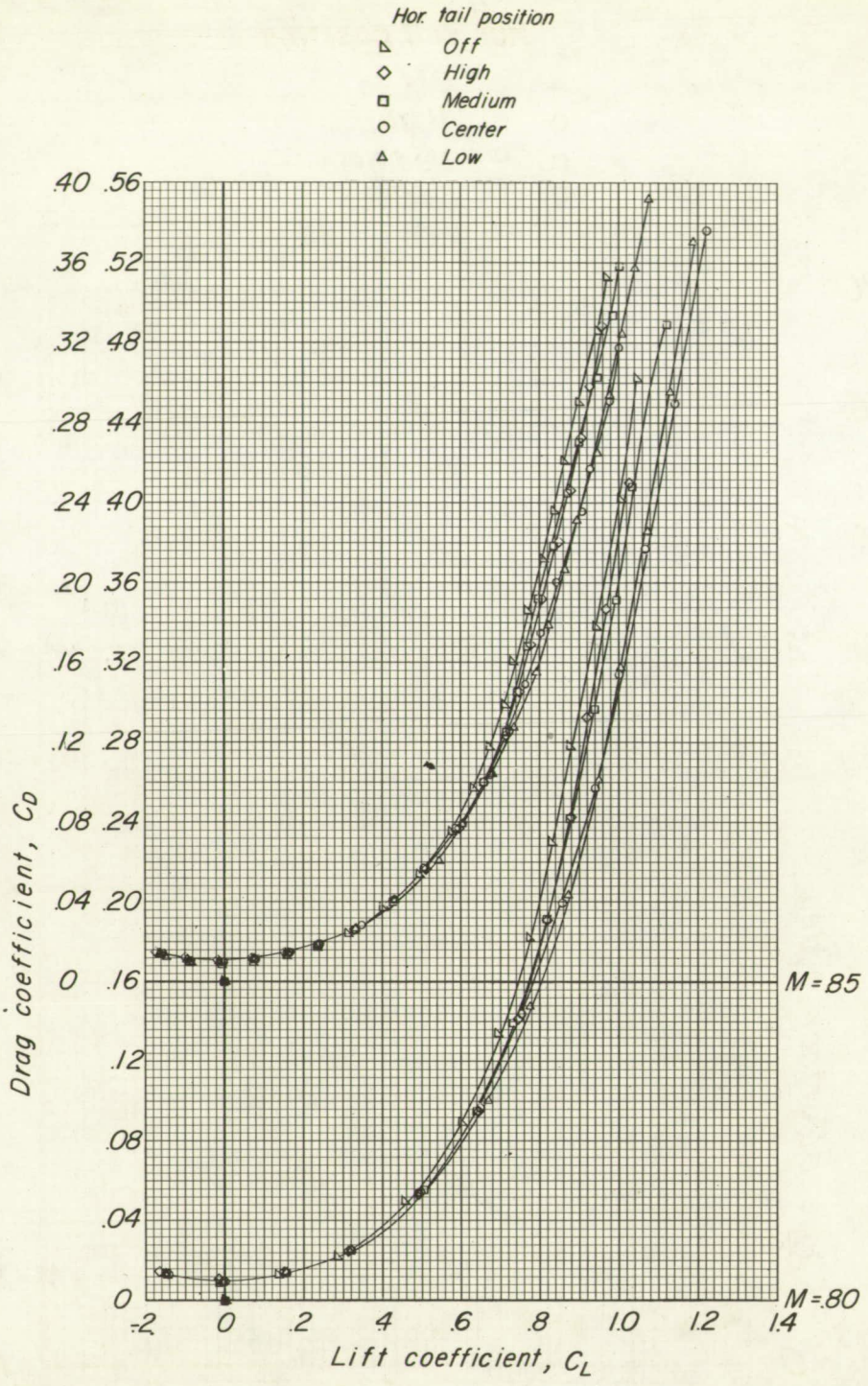

Figure 6.- Variation of drag coefficient with lift coefficient of high-wing—fuselage model without and with horizontal tail at various vertical locations.

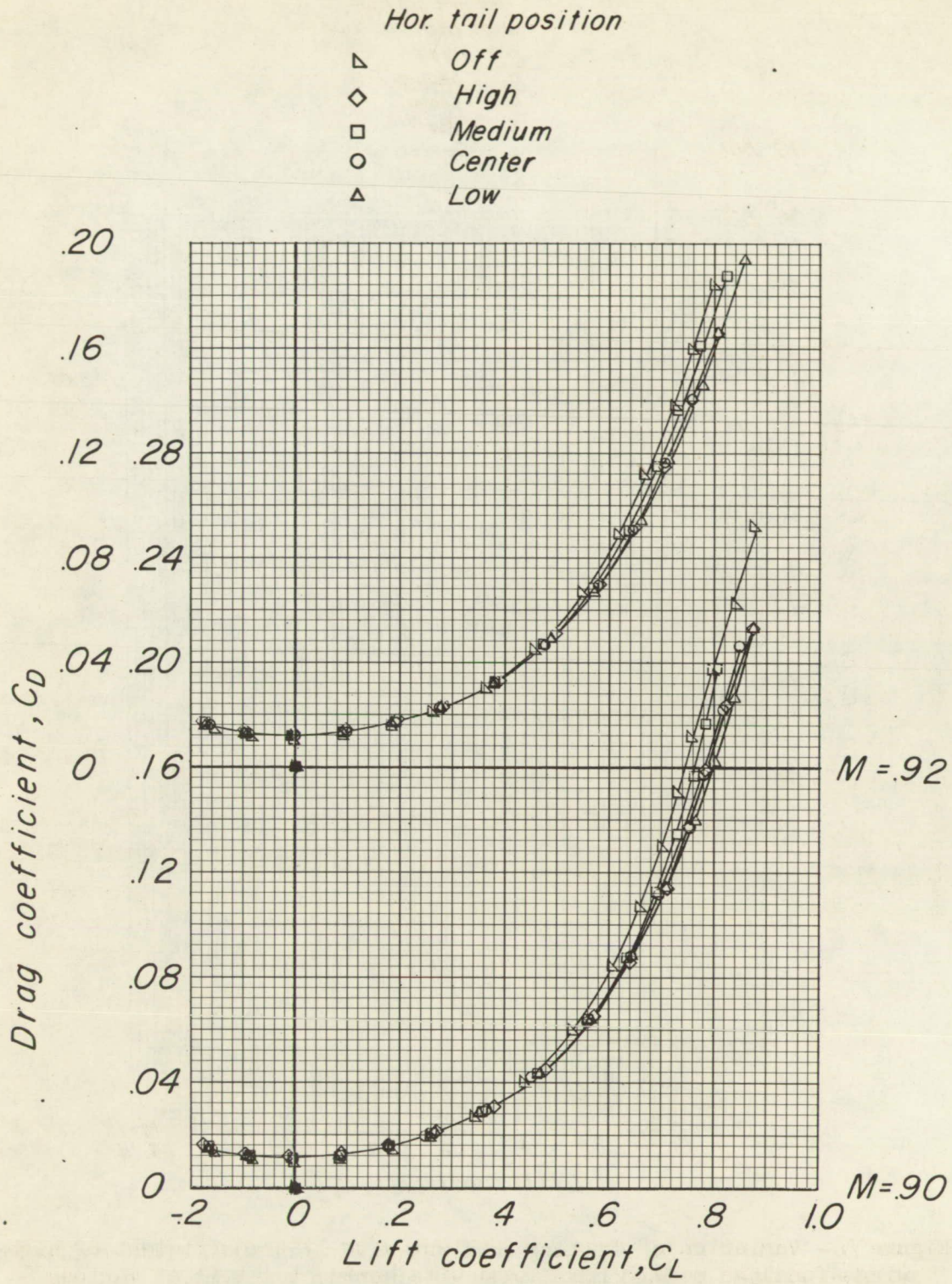

Figure 6.- Concluded.

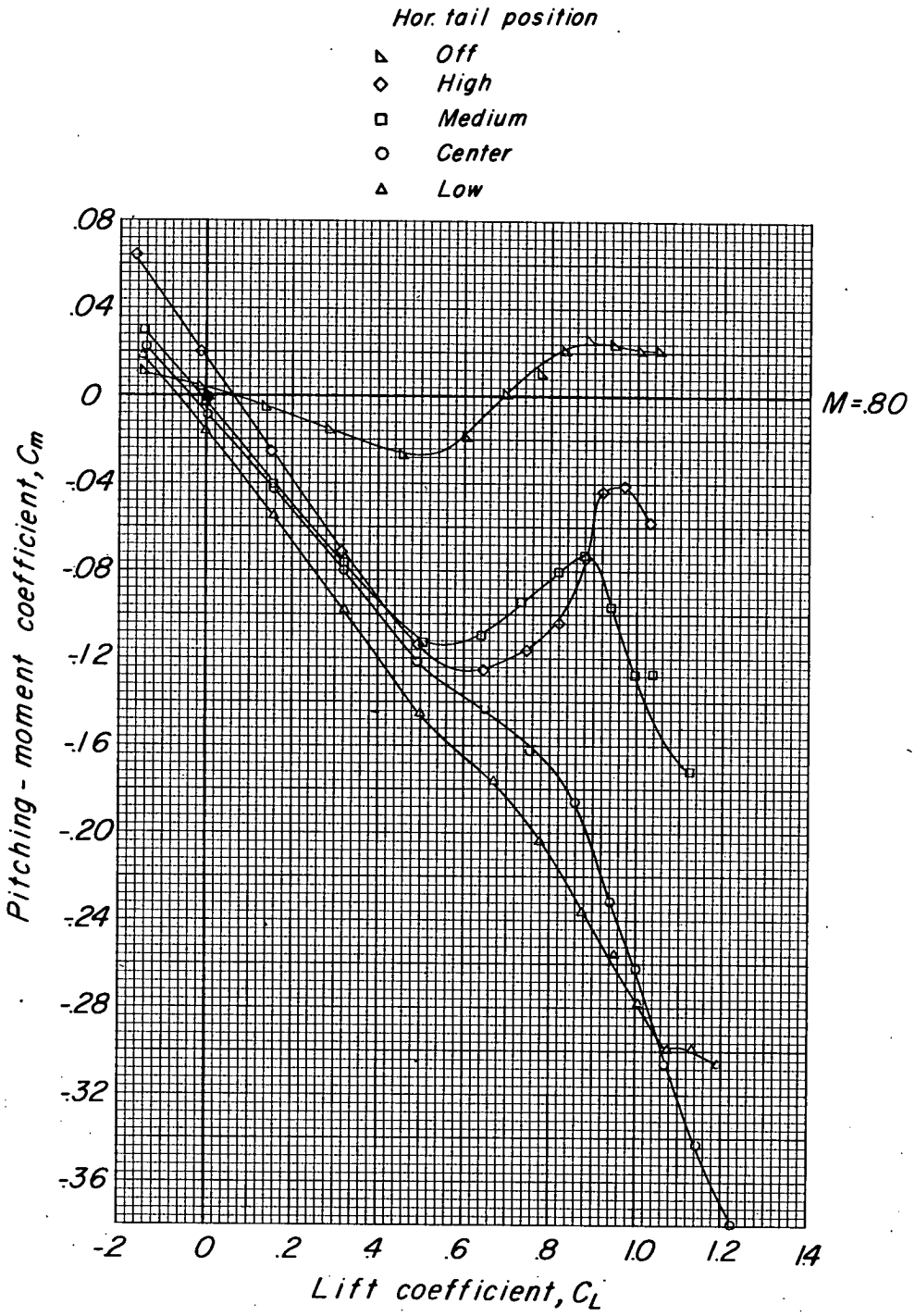

Figure 7.- Variation of pitching-moment coefficient with lift coefficient of high-wing—fuselage model without and with horizontal tail at various vertical locations.

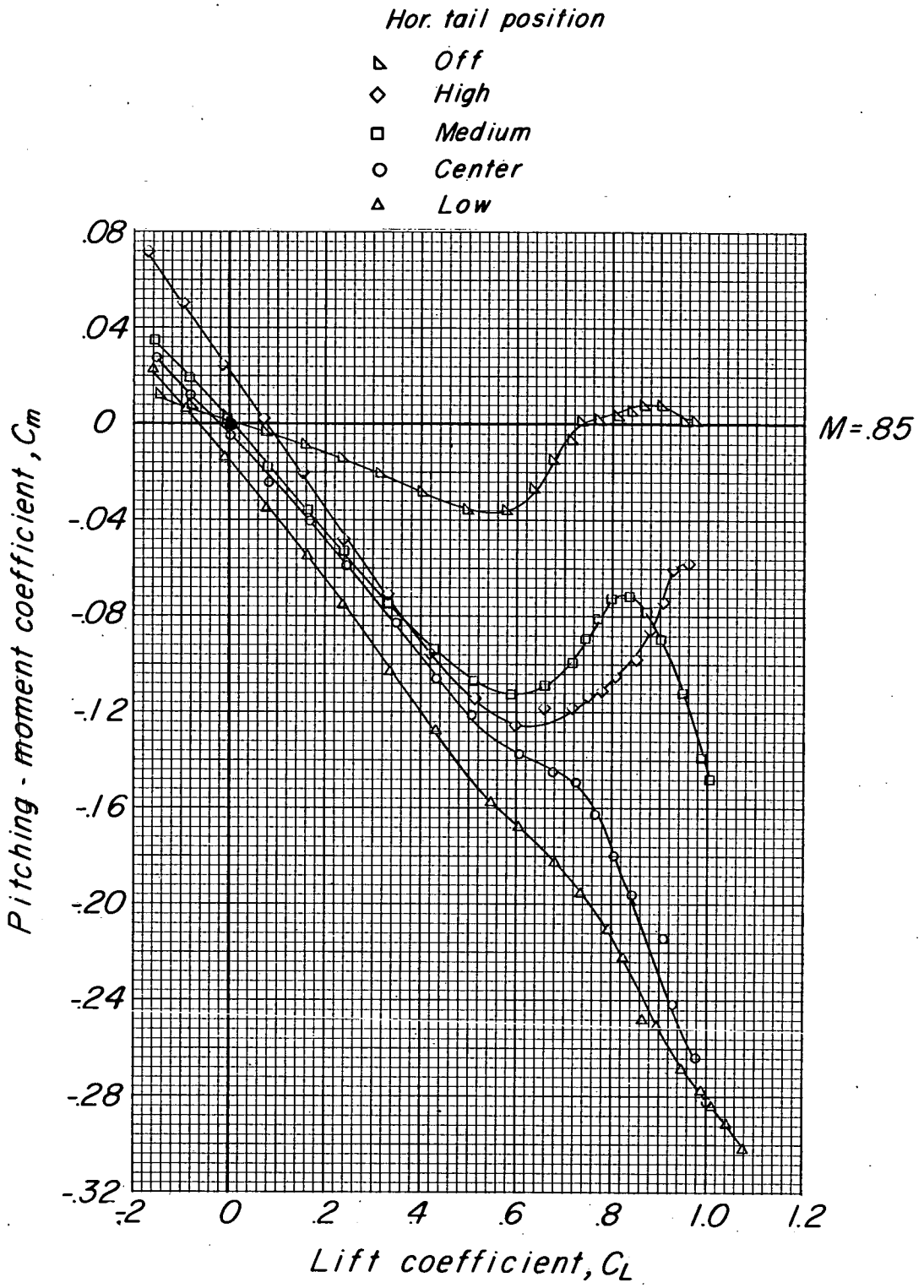

Figure 7.- Continued.

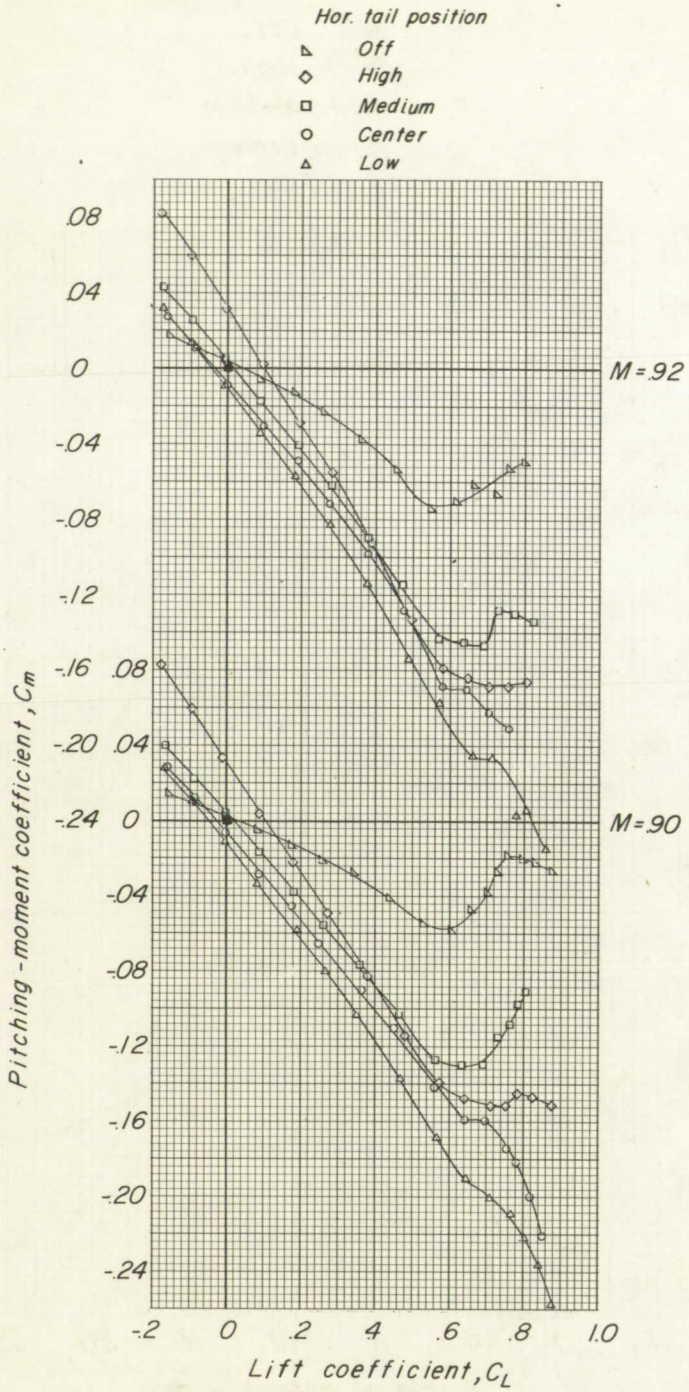

Figure 7.- Concluded.

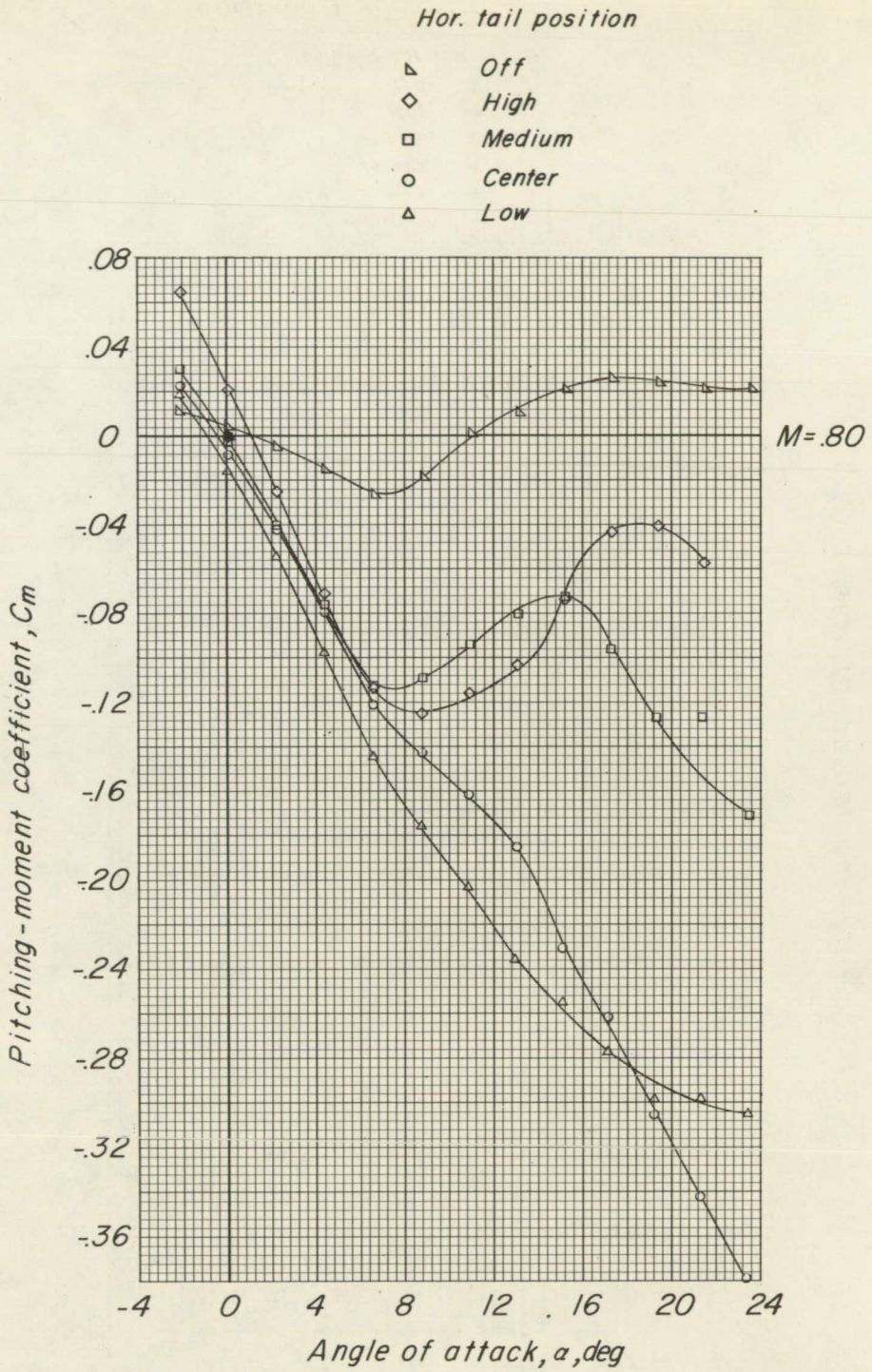

Figure 8.- Variation of pitching-moment coefficient with angle of attack of high-wing—fuselage model without and with horizontal tail at various vertical locations.

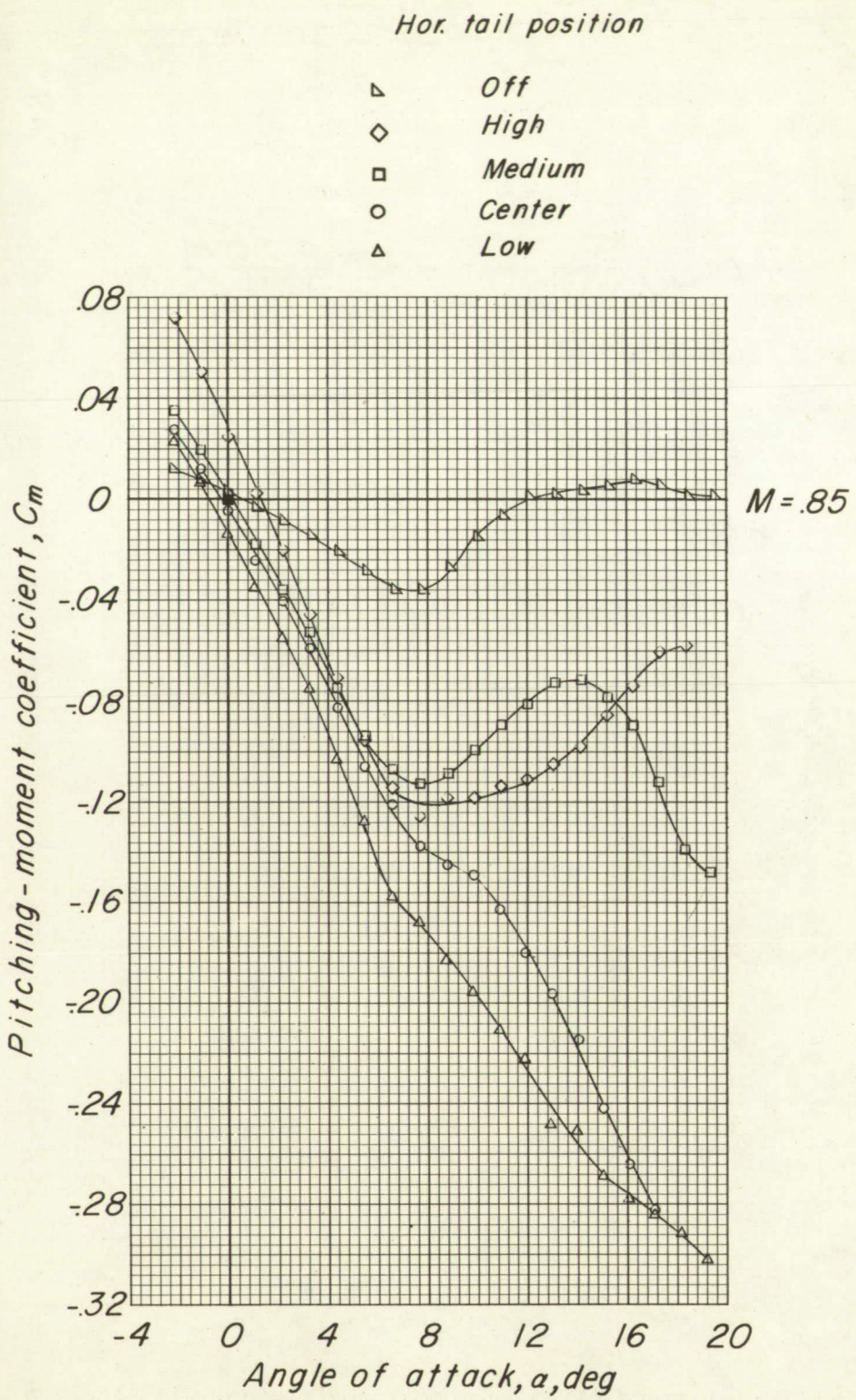

Figure 8.- Continued.

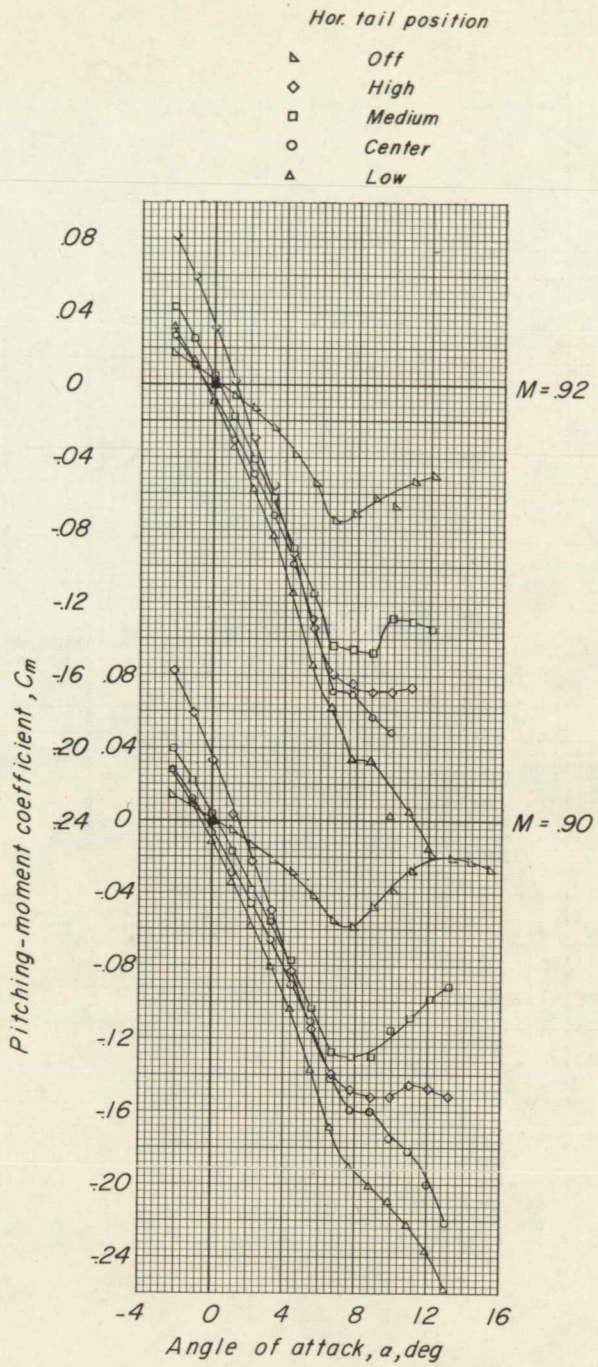

Figure 8.- Concluded.

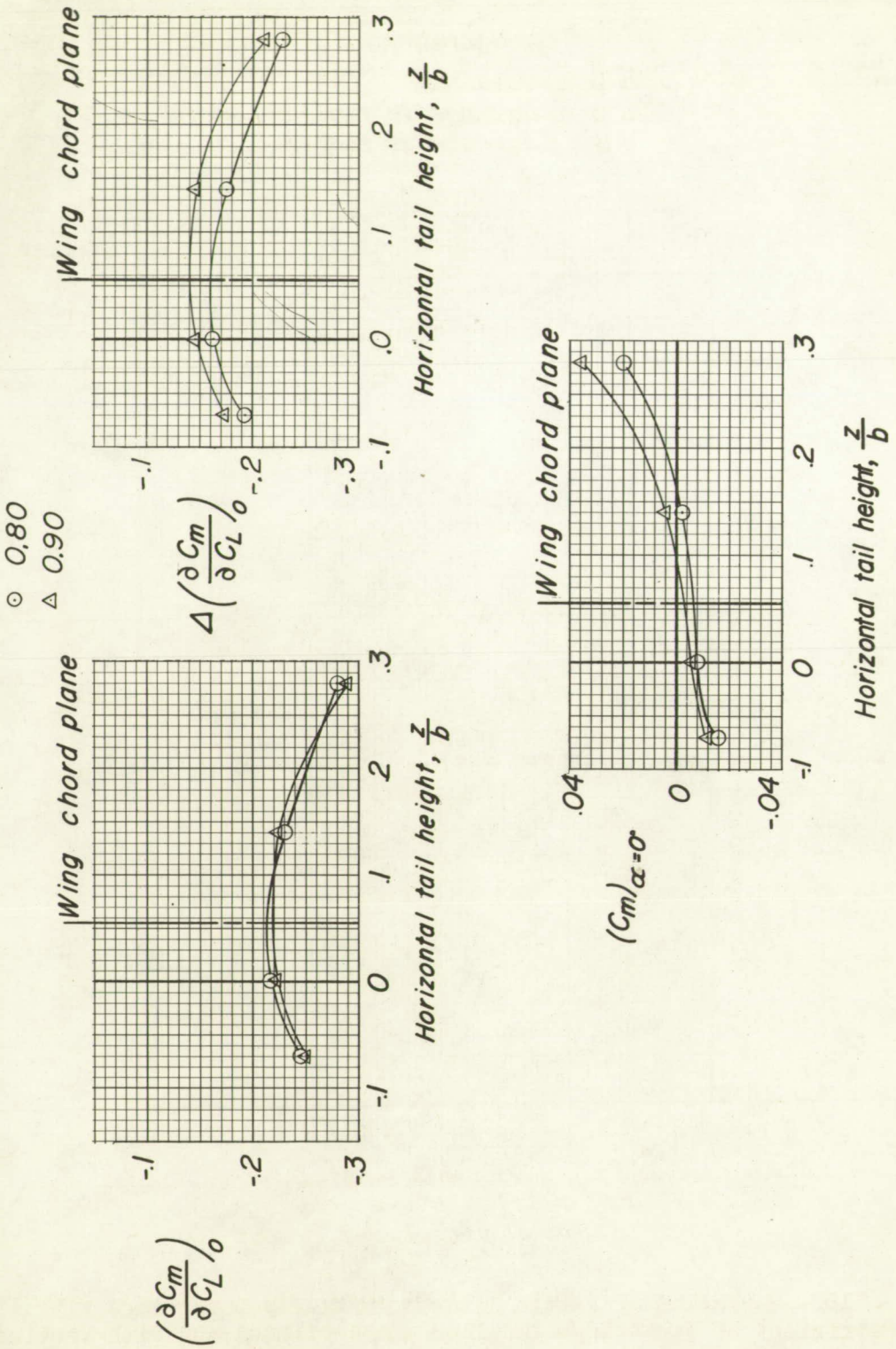

Figure 9.- Effect of tail height on longitudinal stability parameters.

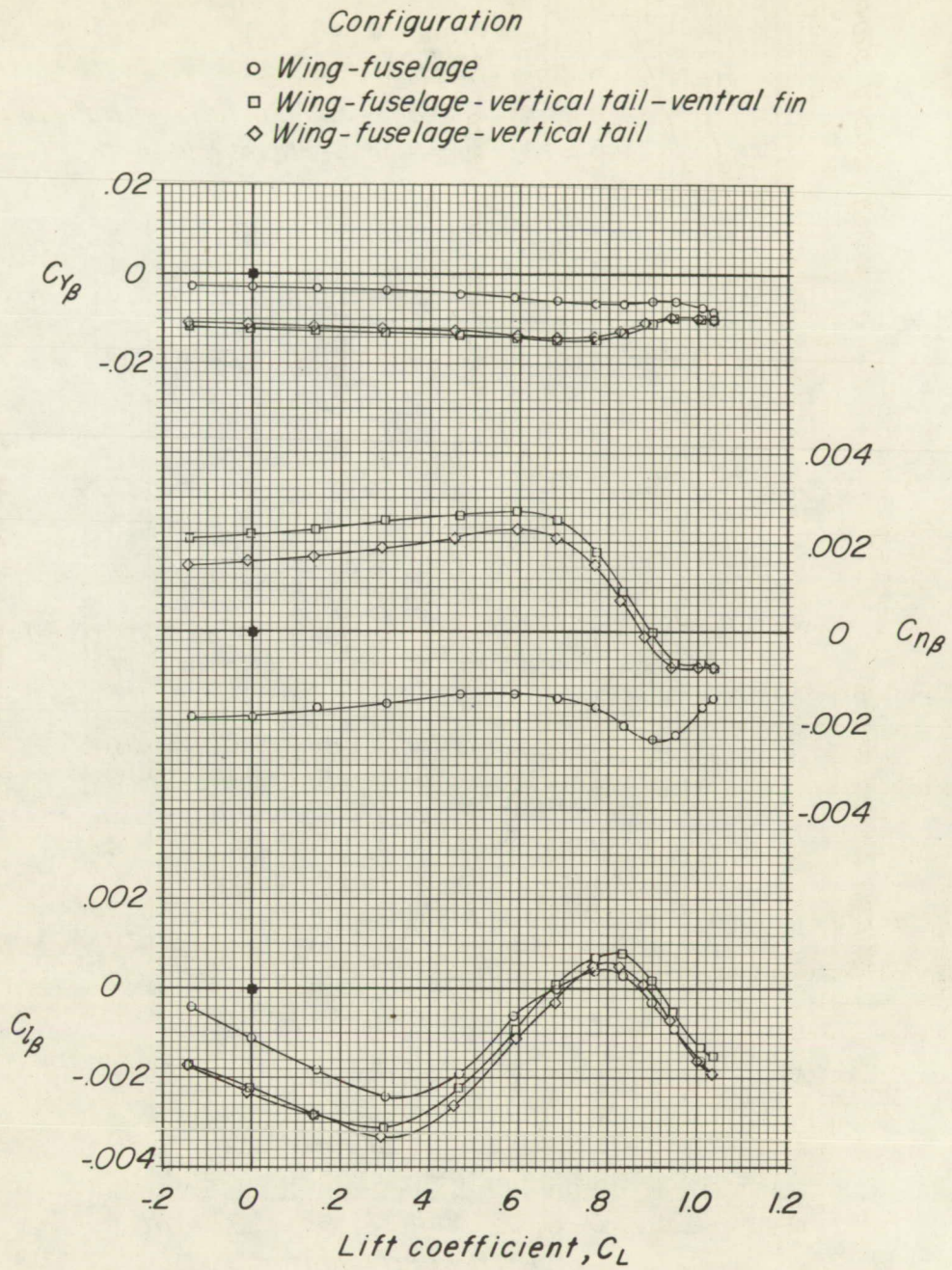

(a) M = 0.80.

Figure 10.- Variation of static lateral stability parameters with lift coefficient of high-wing—fuselage model without and with vertical tail.

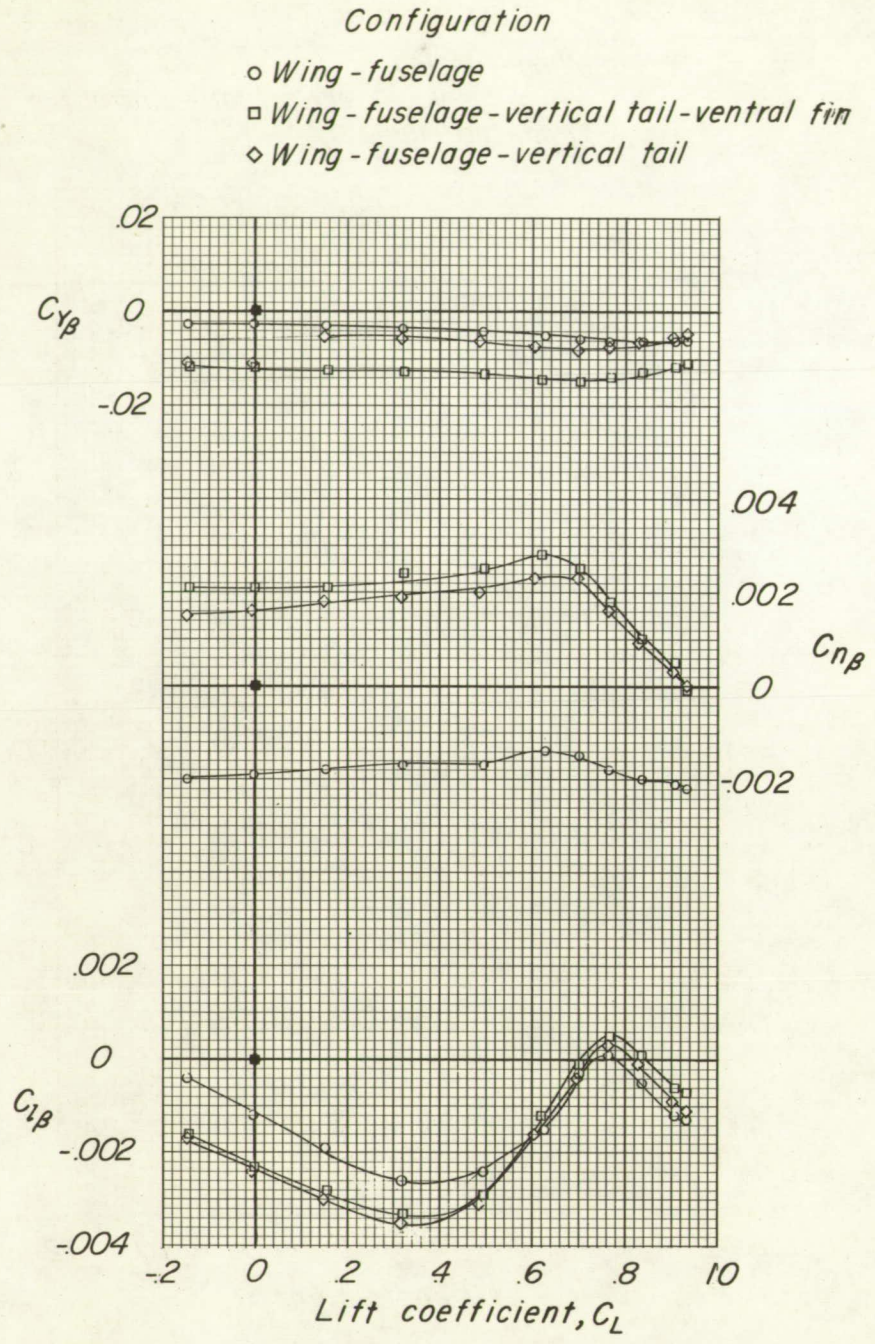

(b) M = 0.85.

Figure 10.- Continued.

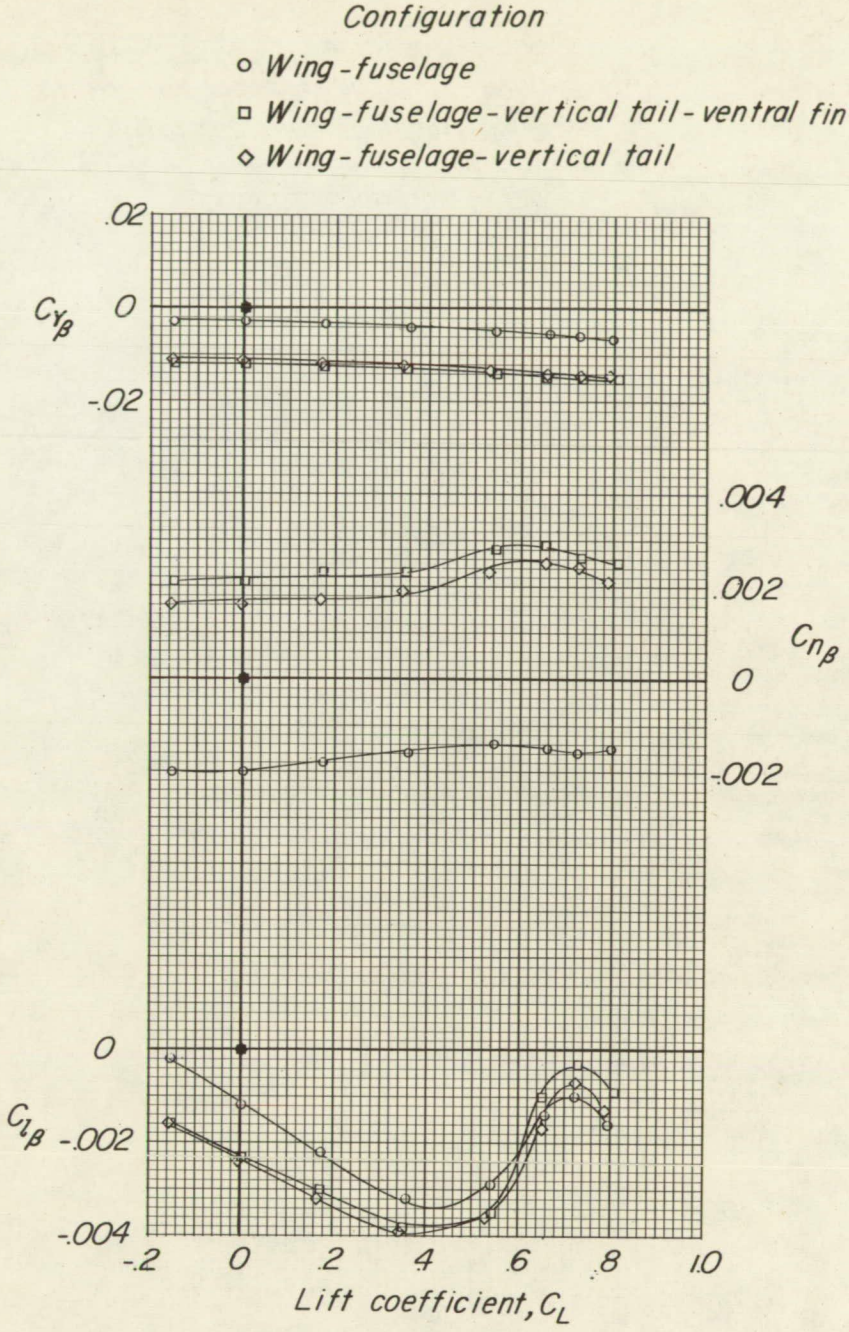

(c) M = 0.90.

Figure 10.- Continued.

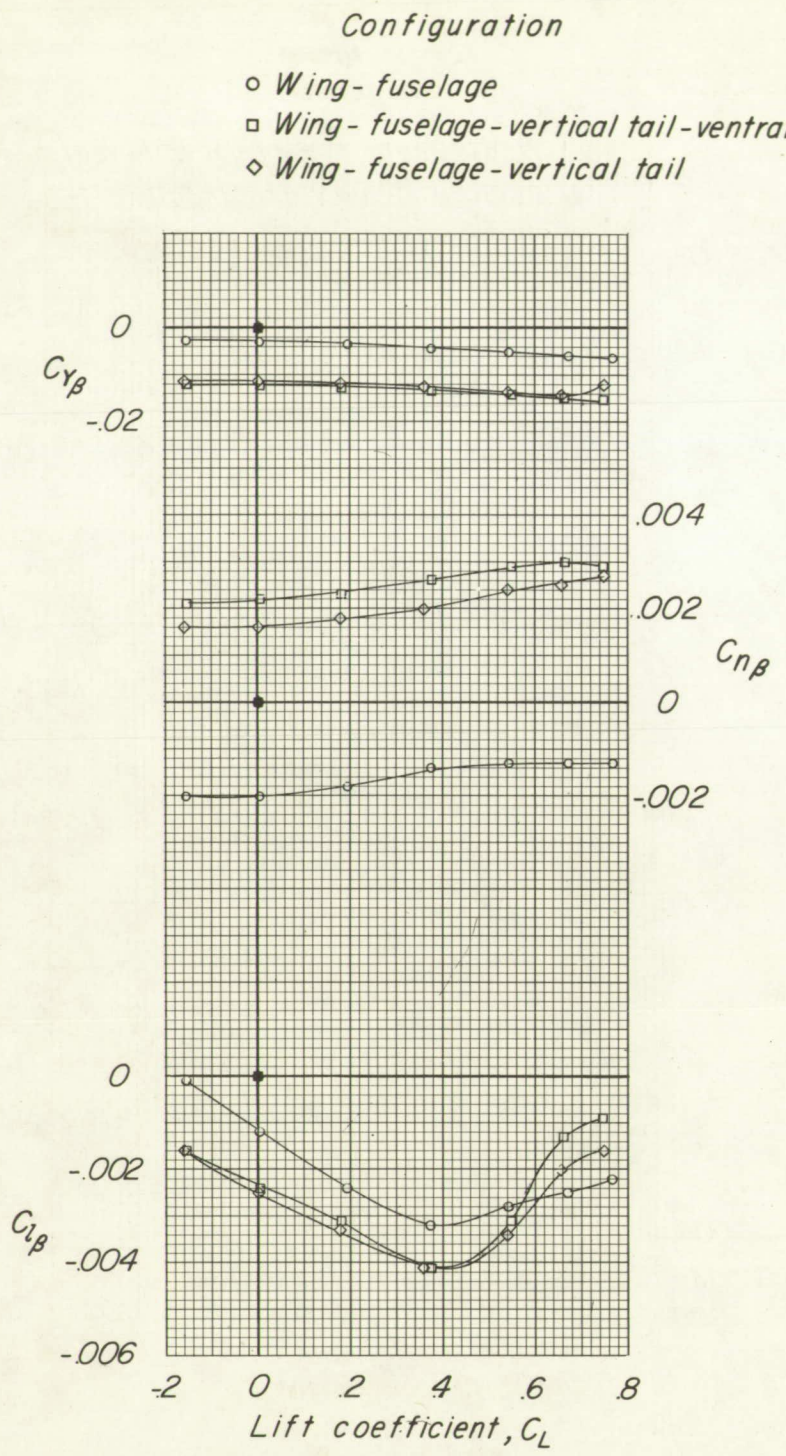

(d) M = 0.92.

Figure 10.- Concluded.

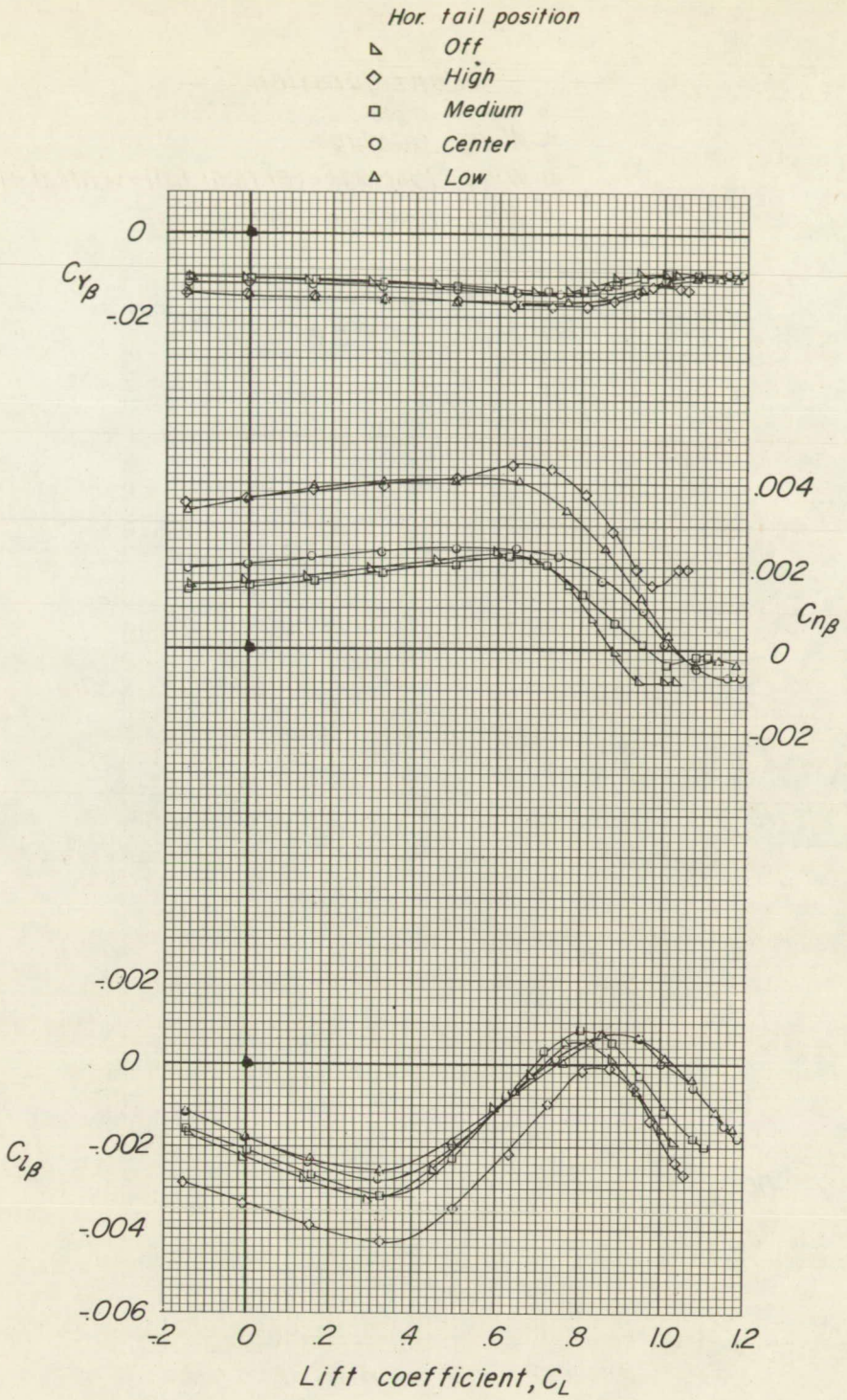

(a) M = 0.80.

Figure 11.- Variation of static lateral stability parameters with lift coefficient of high-wing—fuselage model without and with horizontal tail at various vertical locations.

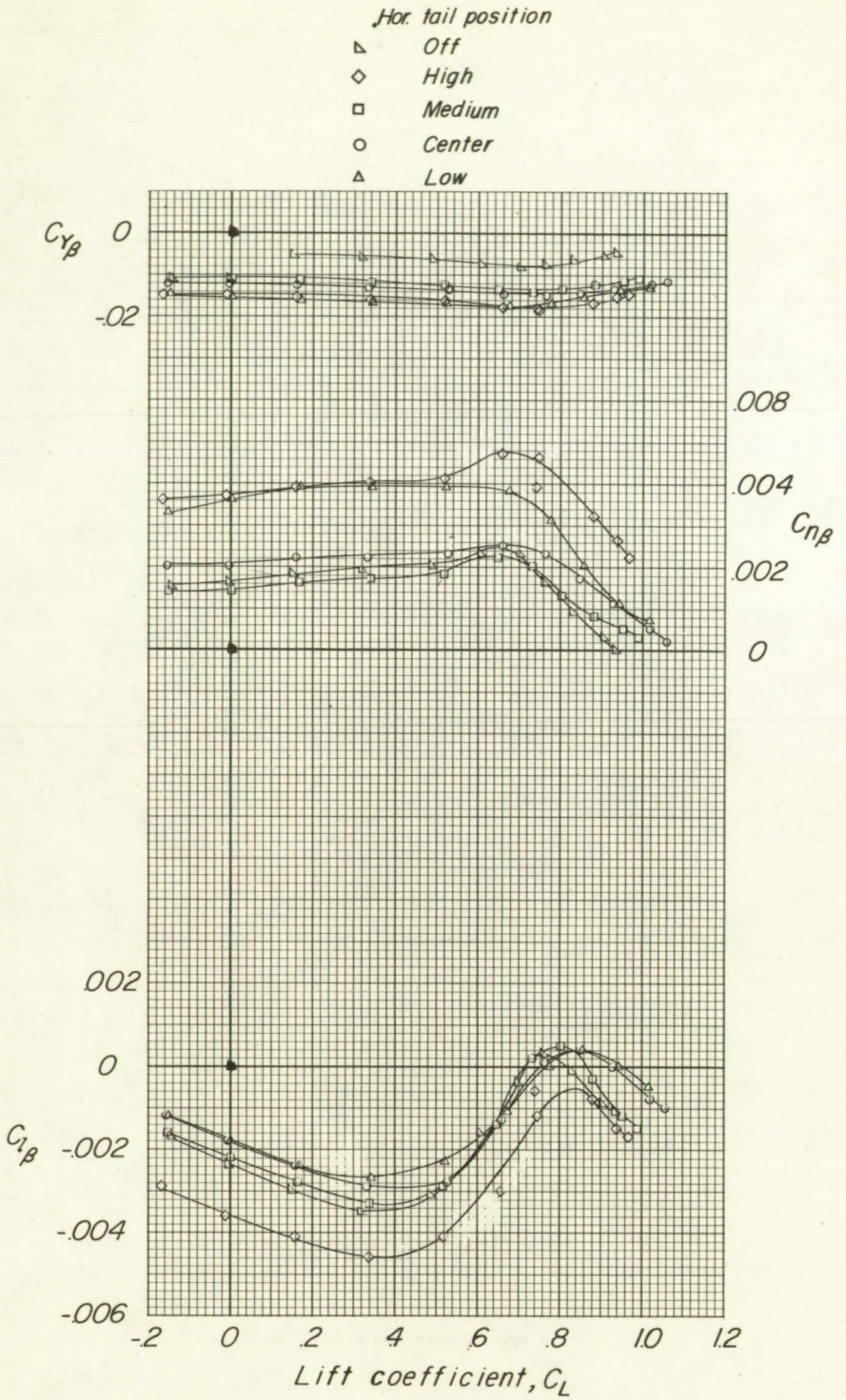

(b) M = 0.85.

Figure 11.- Continued.

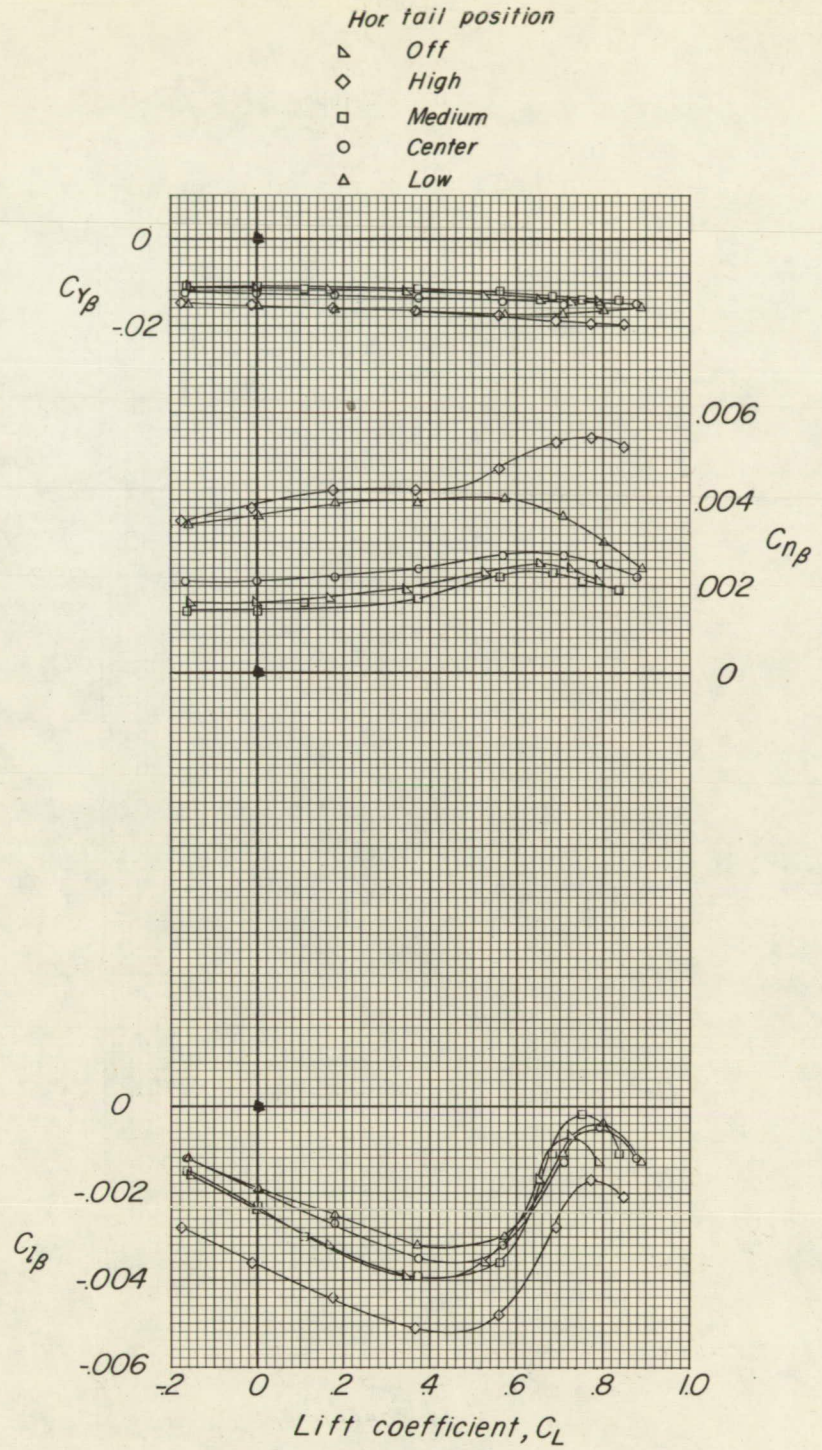

(c) M = 0.90.

Figure 11.- Continued.

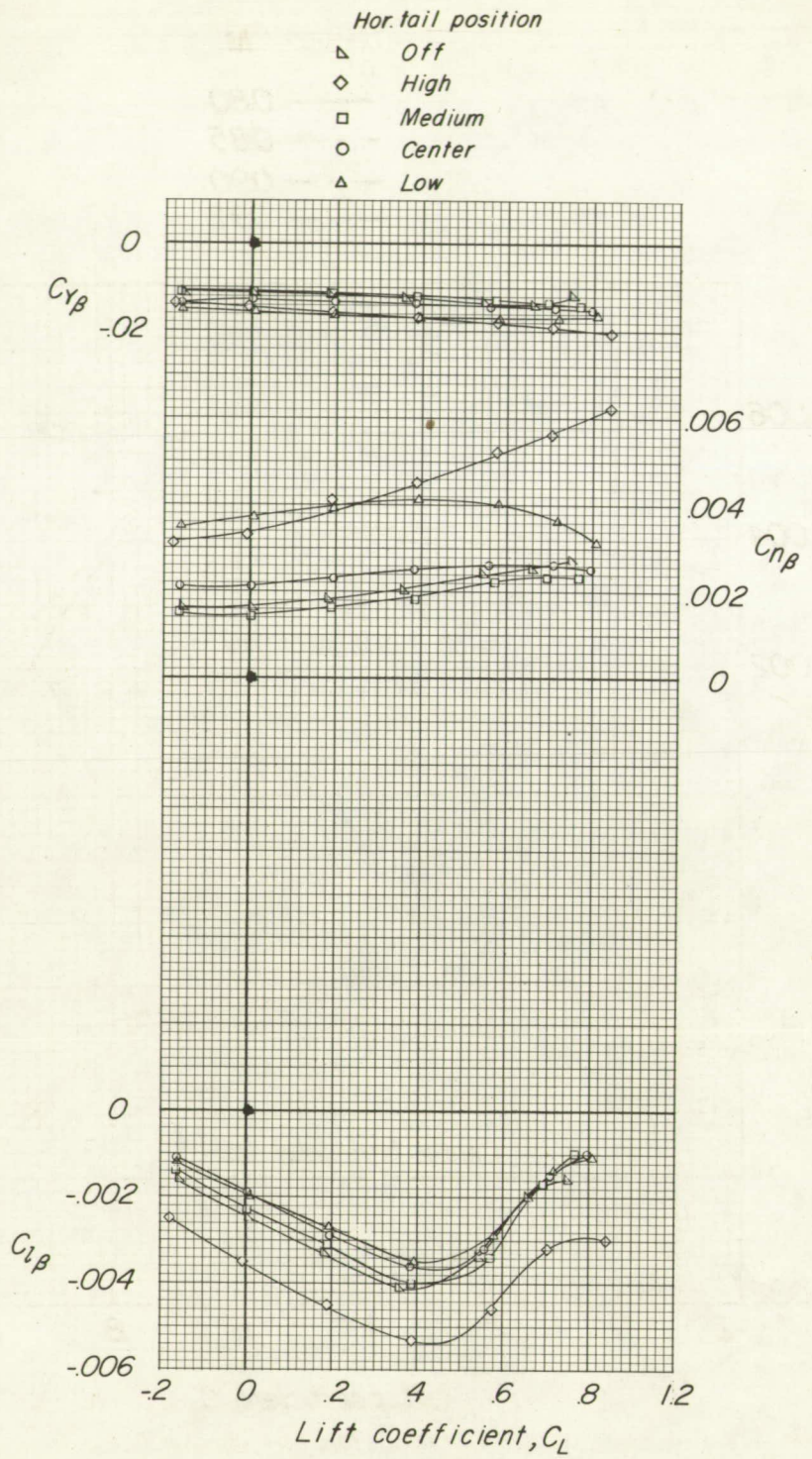

(d) M = 0.92.

Figure 11.- Concluded.

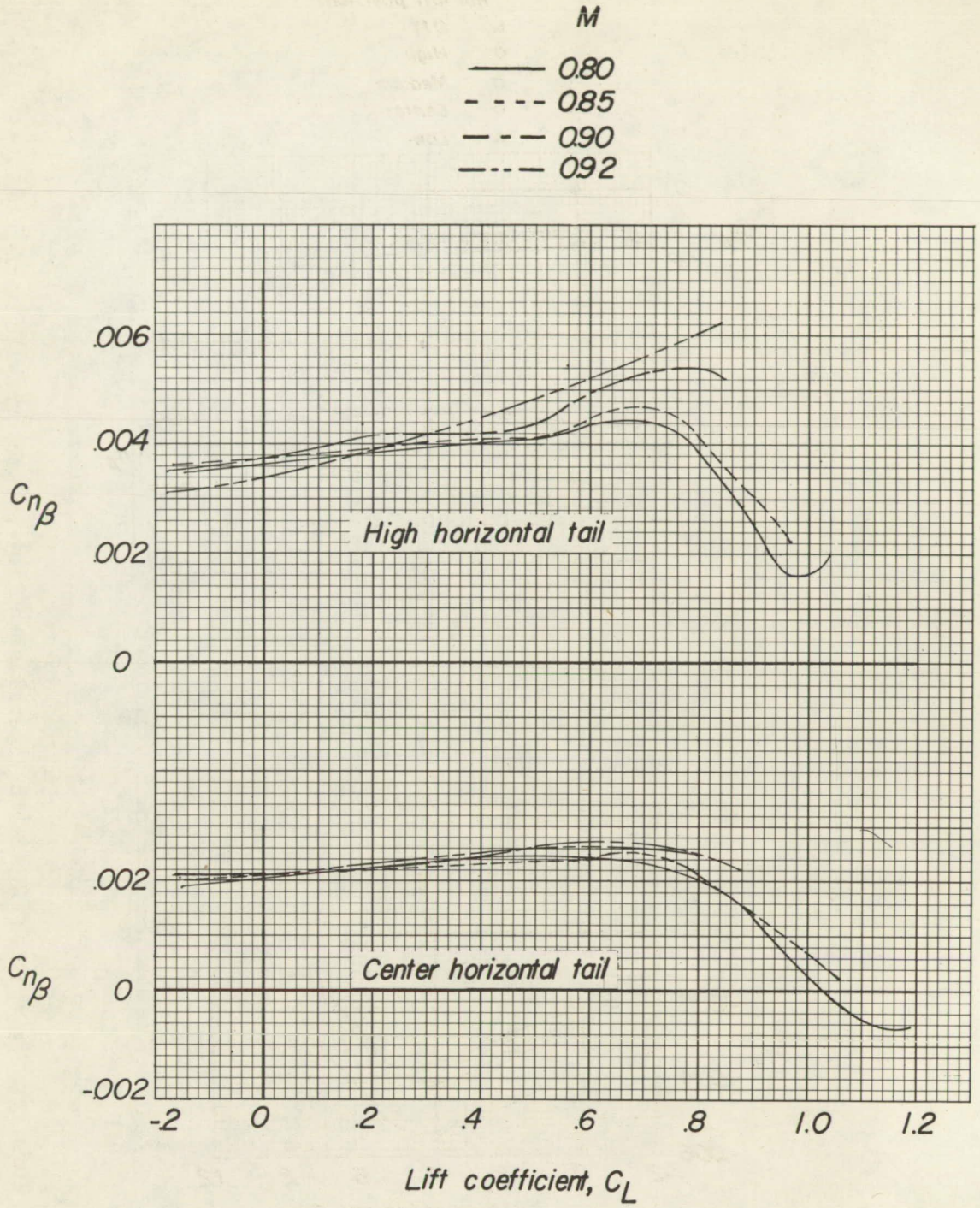

Figure 12.- Effect of Mach number on the variation of C_{n_β} with C_L for two horizontal-tail locations.

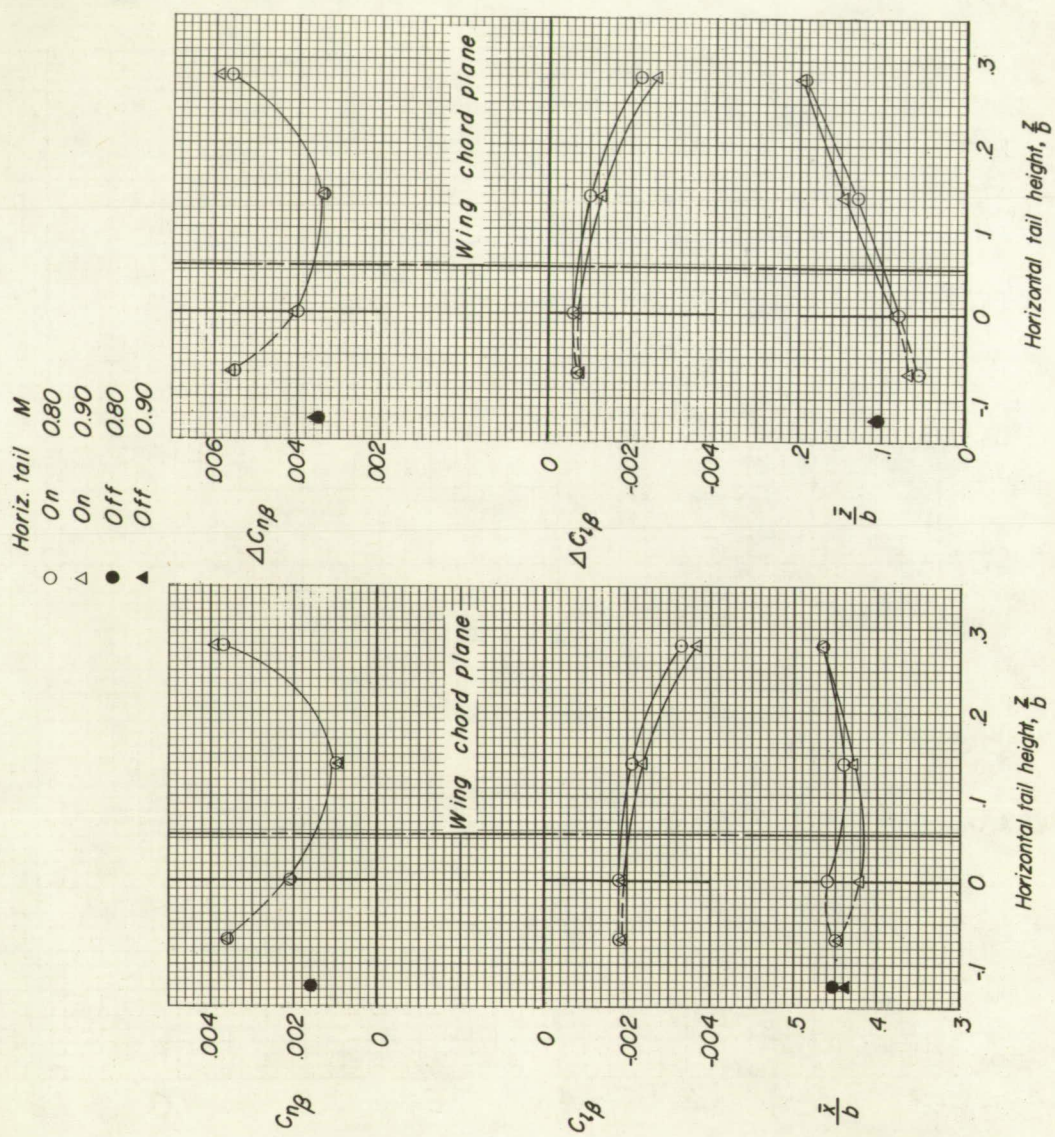

Figure 13.- Summary of variation of static-lateral stability parameters with horizontal-tail height at low lift coefficients.

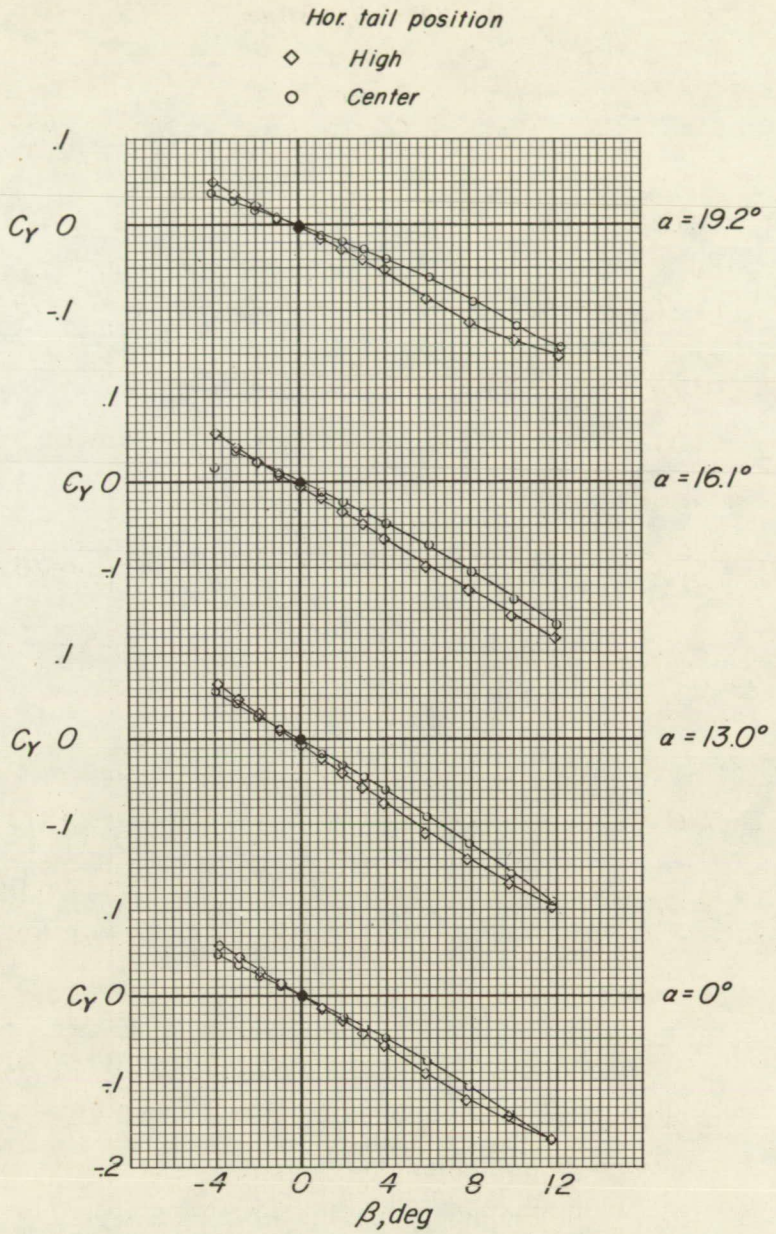

(a) C_Y against β.

Figure 14.- Variation of lateral aerodynamic characteristics with angle of sideslip at various angles of attack of high-wing—fuselage model with horizontal tail in center and high positions. M = 0.80.

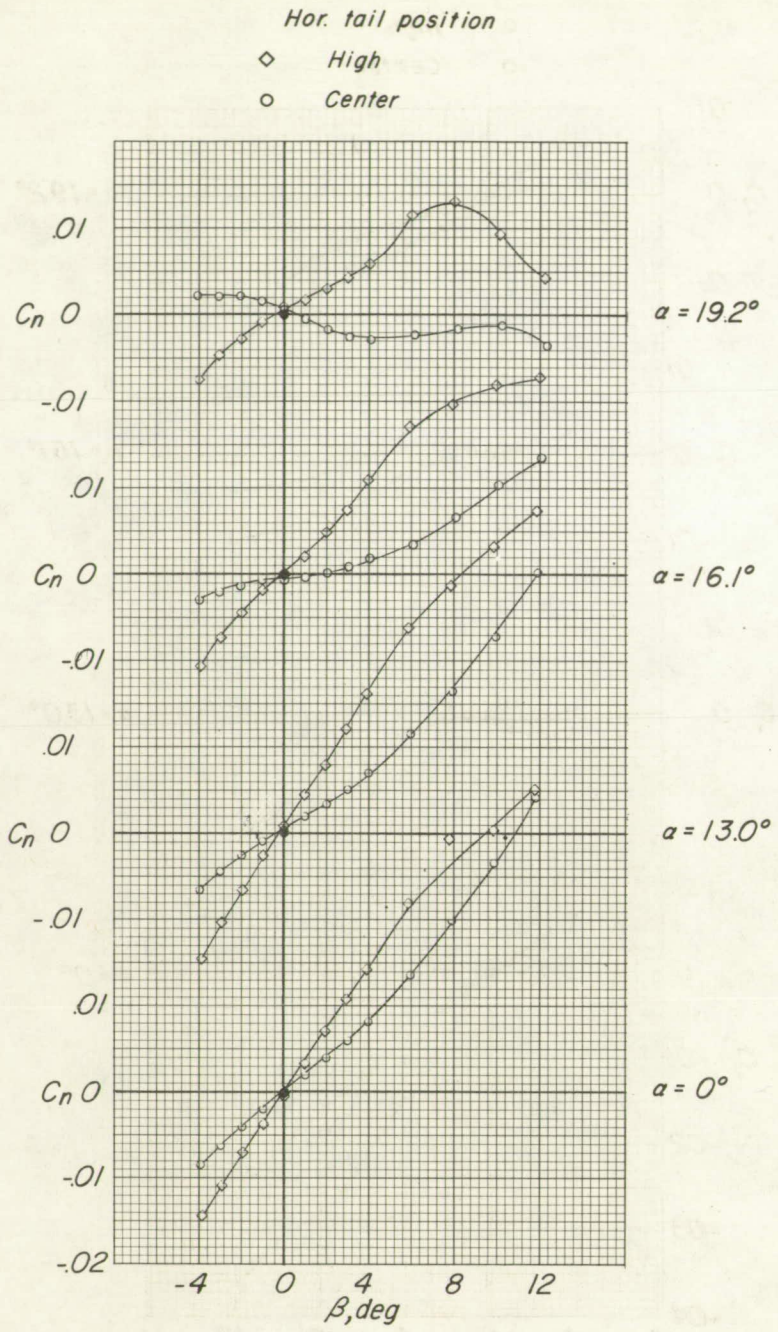

(b) C_n against β.

Figure 14.- Continued.

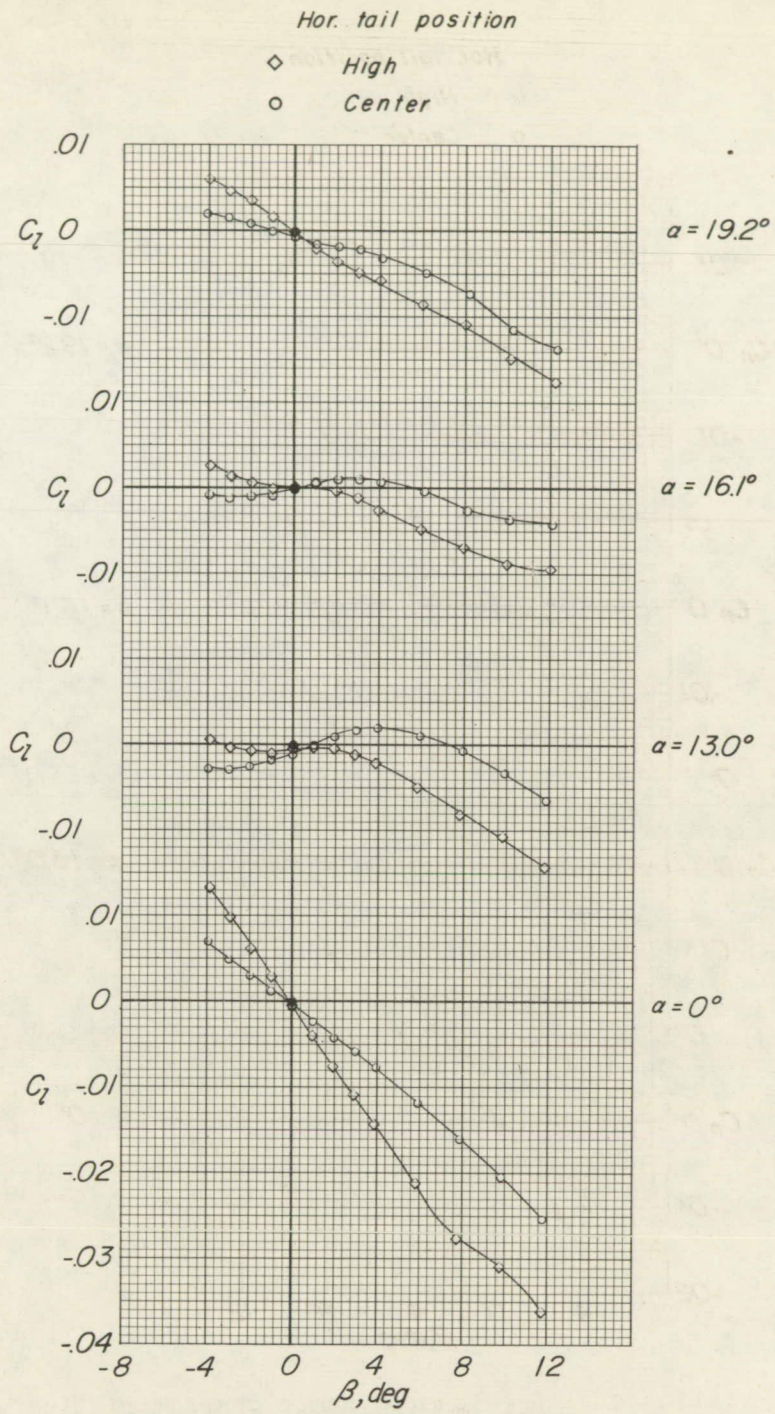

(c) C_l against β.

Figure 14.- Concluded.

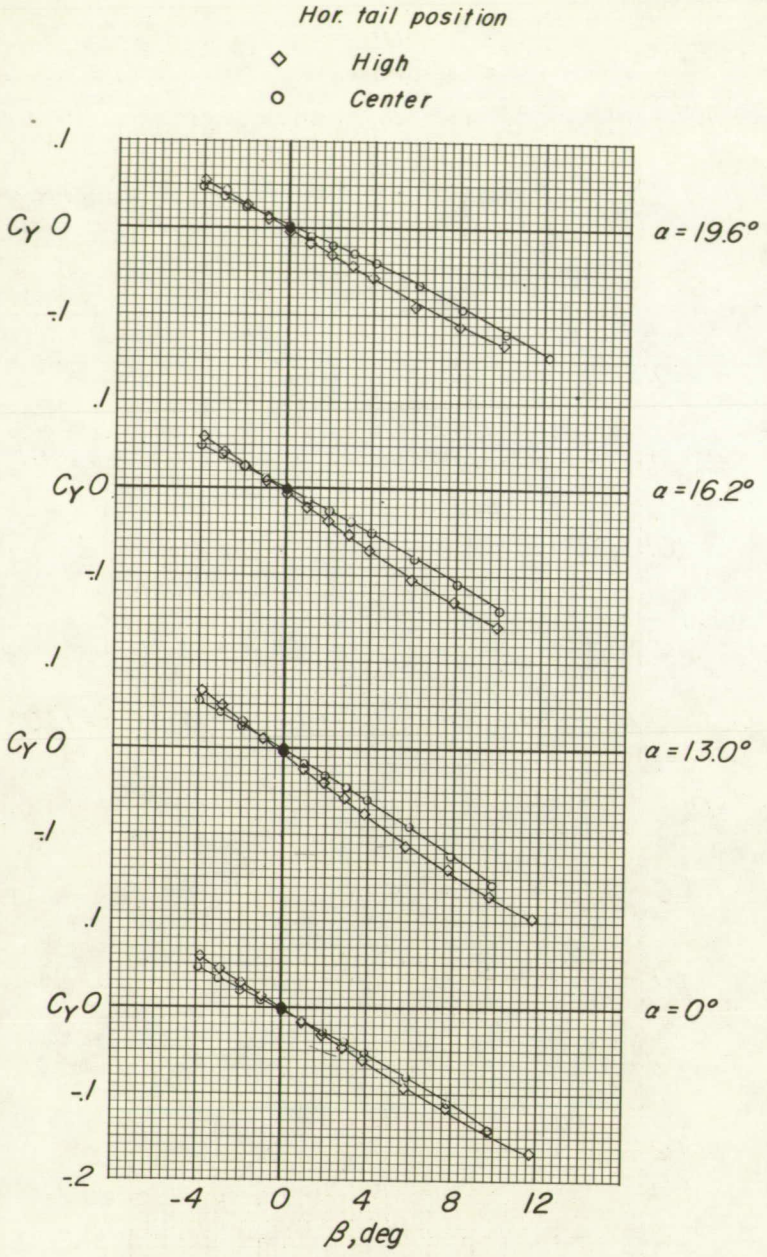

(a) C_Y against β.

Figure 15.- Variation of lateral aerodynamic characteristics with angle of sideslip at various angles of attack of high-wing—fuselage model with horizontal tail in center and high positions. M = 0.85.

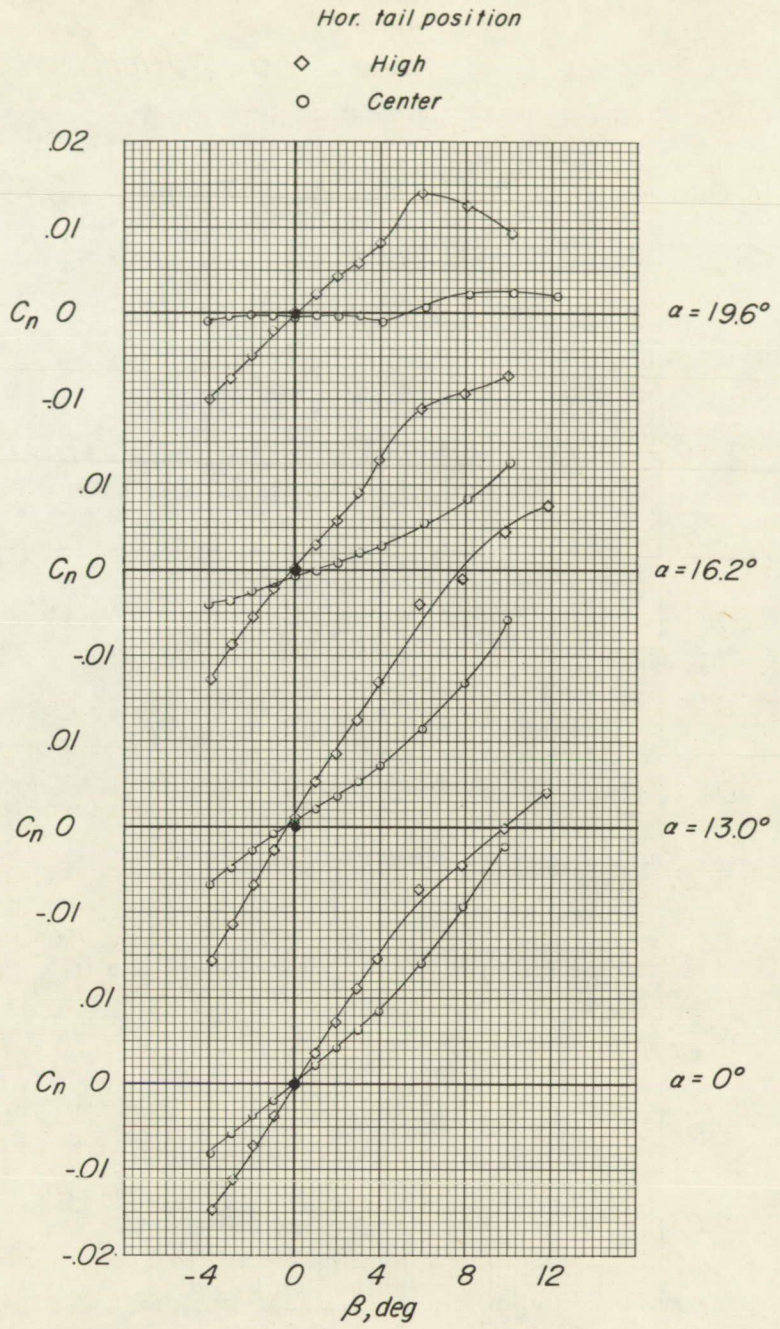

(b) C_n against β.

Figure 15.- Continued.

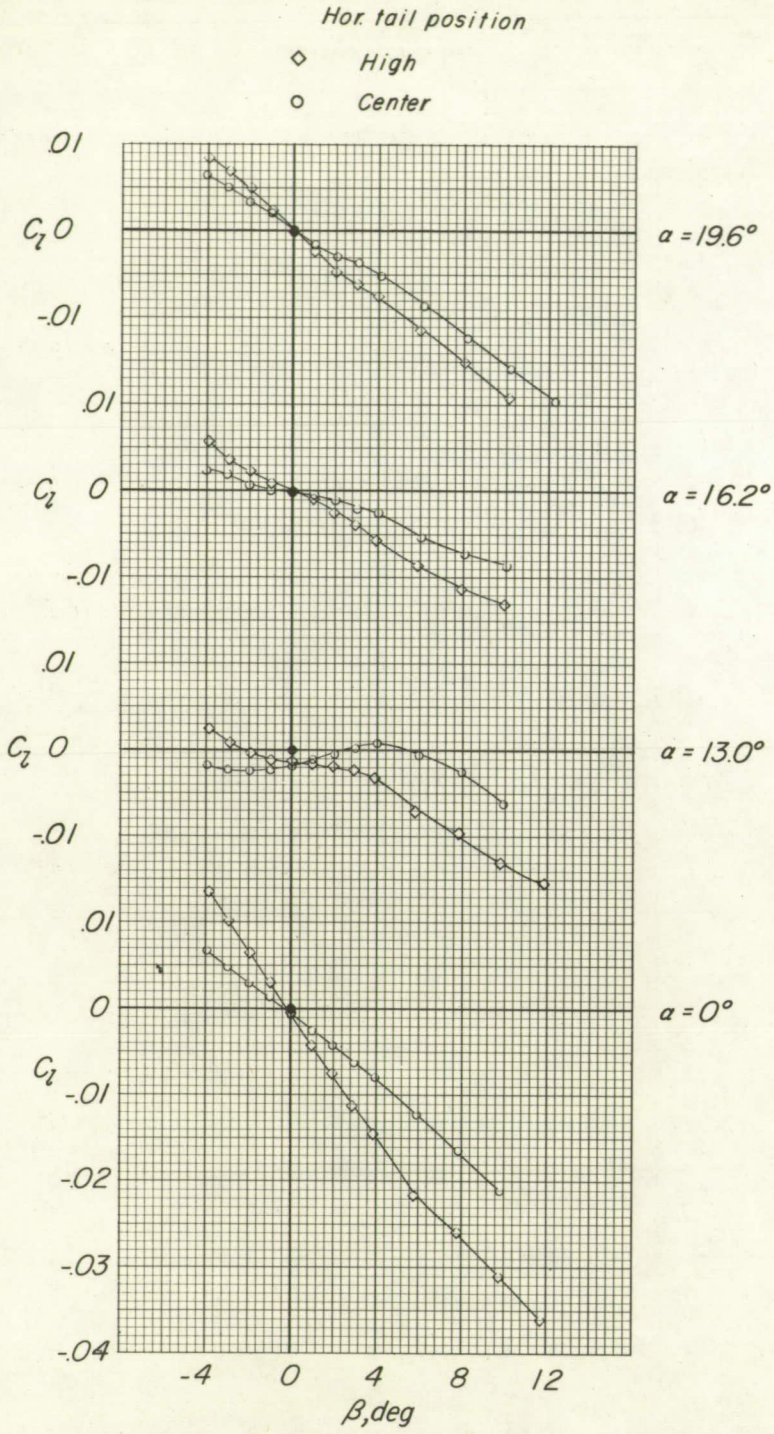

(c) C_l against β.

Figure 15.- Concluded.

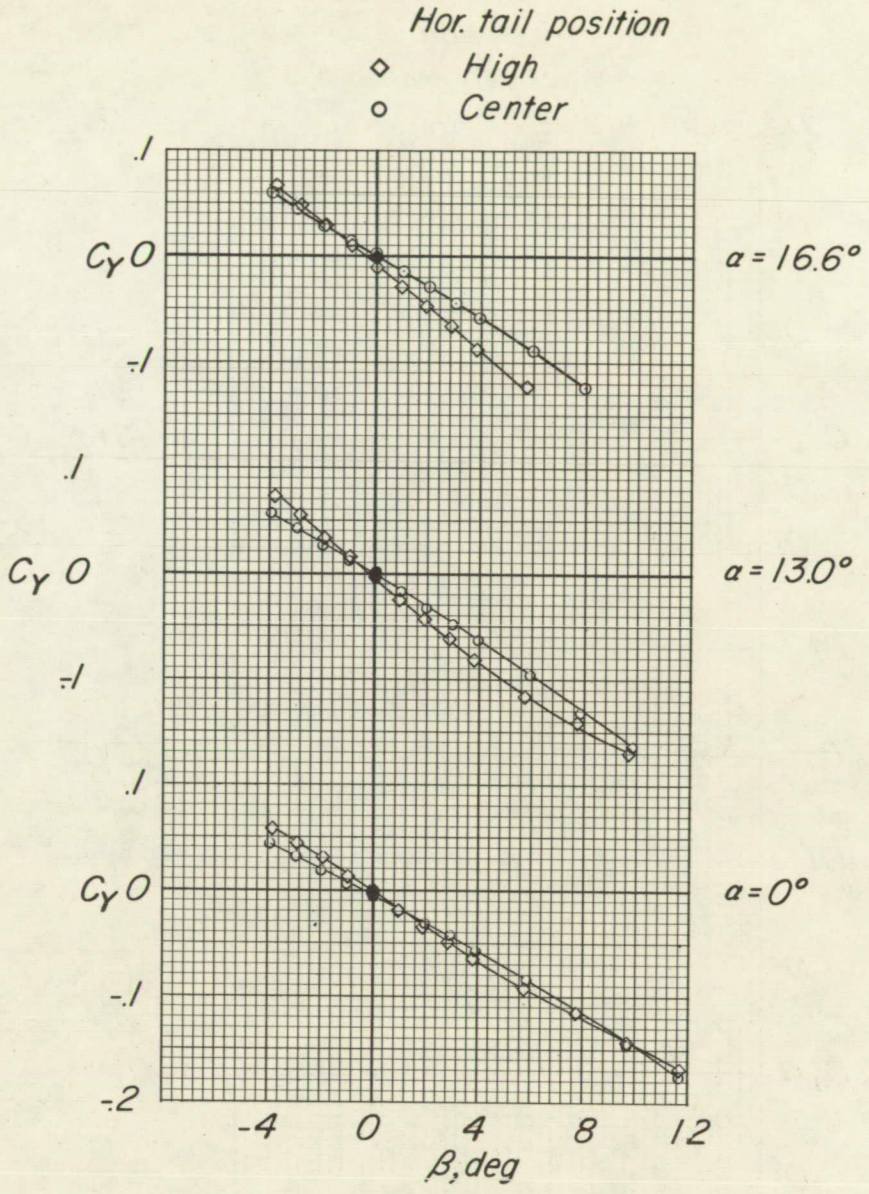

(a) C_Y against β.

Figure 16.- Variation of lateral aerodynamic characteristics with angle of sideslip at various angles of attack of high-wing—fuselage model with horizontal tail in center and high positions. M = 0.90.

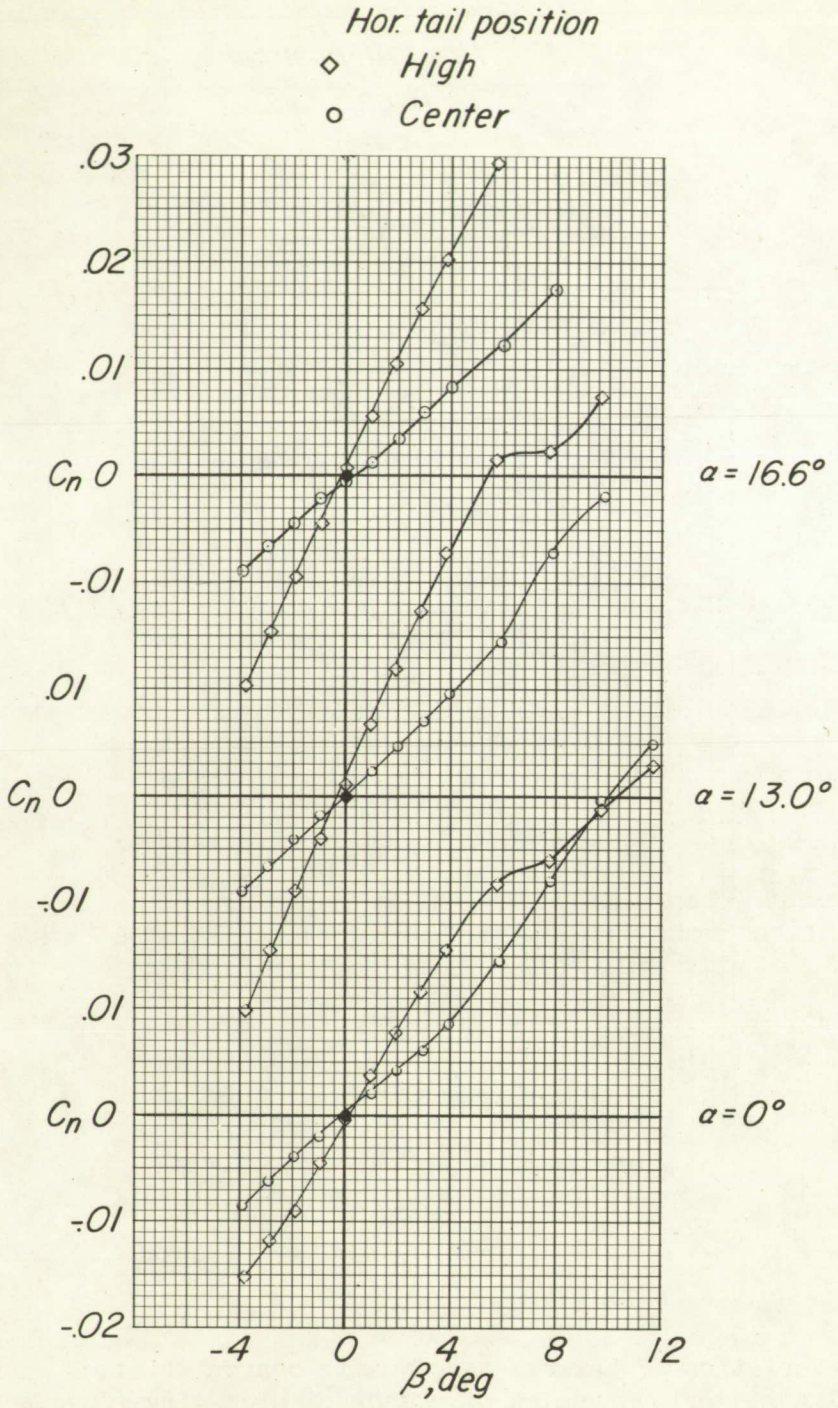

(b) C_n against β.

Figure 16.- Continued.

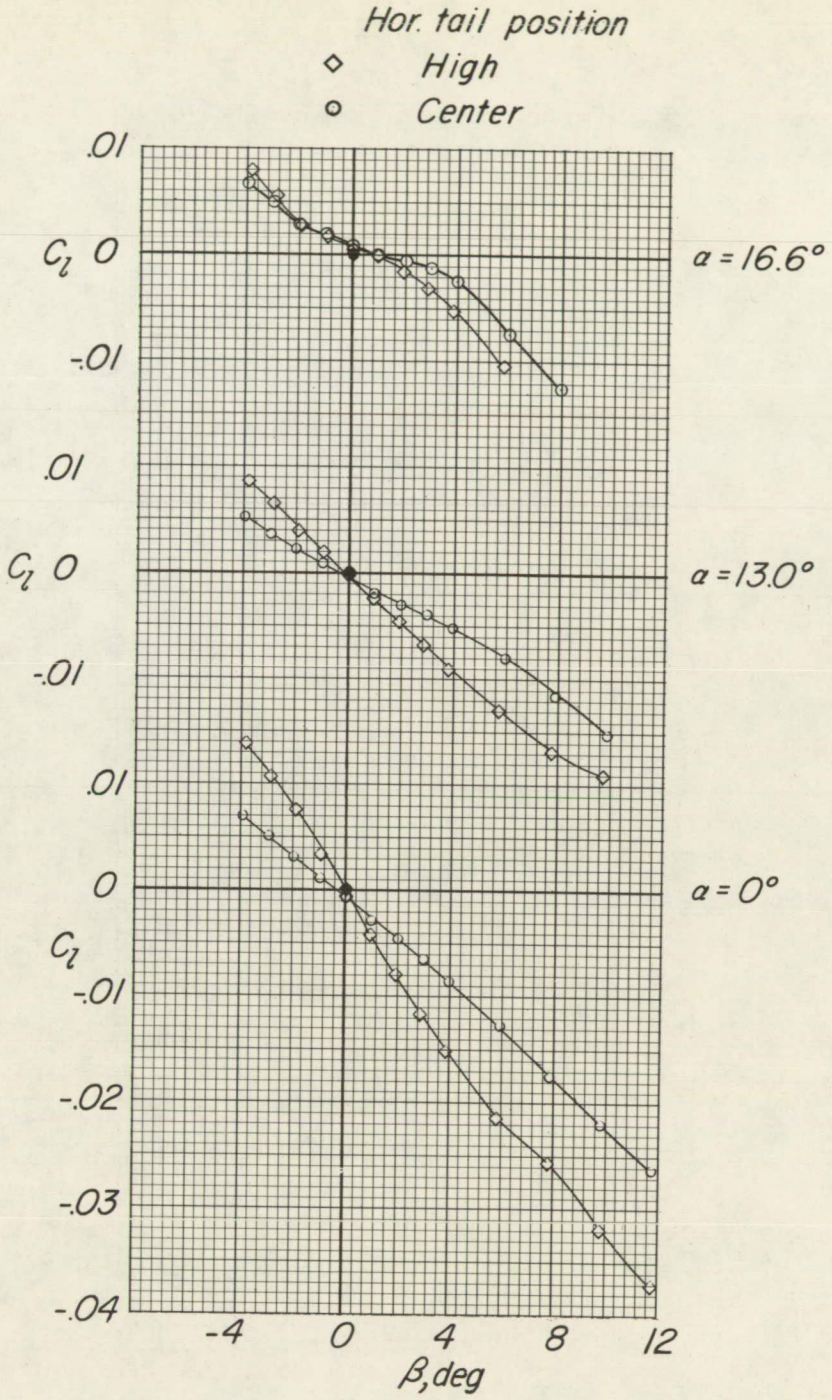

(c) C_l against β.

Figure 16.- Concluded.

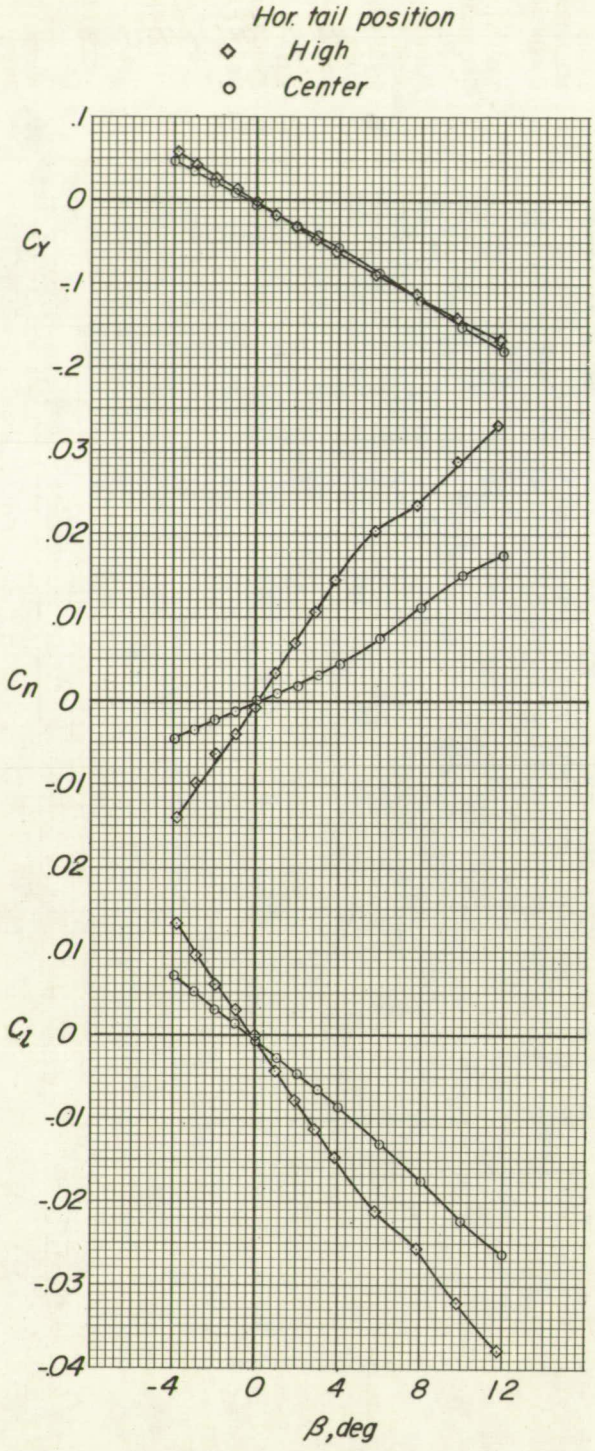

Figure 17.- Variation of lateral aerodynamic characteristics with angle of sideslip of high-wing—fuselage model with horizontal tail in center and high positions. M = 0.92; $\alpha = 0^{o}$.